Interpretation of Galileo's Io plasma and field observations: I0, I24, and I27 flybys and close polar passes

Joachim Saur, Fritz M. Neubauer, Darell Strobel, Michael E. Summers

Interpretation of Galileo's Io plasma and field observations: I0, I24, and I27 flybys and close polar passes

Joachim Saur[1] and Fritz M. Neubauer
Institut für Geophysik u. Meteorologie, Universität zu Köln, Albertus Magnus Platz, Cologne, Germany

Darrell F. Strobel
Departments of Earth and Planetary Sciences and Physics and Astronomy, Johns Hopkins University, Baltimore, Maryland, USA

Michael E. Summers
School of Computational Sciences and Department of Physics and Astronomy, George Mason University, Fairfax, Virginia, USA

Received 4 August 2001; revised 25 April 2002; accepted 14 May 2002; published 4 December 2002.

[1] We interpret plasma and magnetic field observations taken during the Galileo spacecraft Io flybys I0 in December 1995, I24 in October 1999, and I27 in February 2000, and we give predictions for a generic pass over Io's northern pole with a three-dimensional, two-fluid plasma model. We show that all previous field and plasma observations by the Galileo spacecraft can be explained without the assumption of an internal magnetic field of Io in contrast to claims by *Kivelson et al.* [1996a, 1996b] and *Khurana et al.* [1997]. We are also able to reproduce both the magnitude and the structure of the double-peak magnetic field signature of the I0 flyby. The origin of this structure can be attributed to diamagnetic and inertia currents. Observations by a polar flyby should answer Io's internal magnetic field question decisively. We also study the effect of different neutral atmosphere models on Io's electrodynamic interaction. Our analysis suggests that Io's atmosphere is longitudinally asymmetric with the scale height on the upstream side smaller than on the downstream side due to the drag force of the flowing plasma on Io's atmosphere. We also show how the Hall effect in Io's ionosphere generates rotated Alfvén wings. In addition, the high-energy electrons observed by *Williams et al.* [1996, 1999] and *Frank and Paterson* [1999] might play an important role for the formation of Io's downstream wake. *INDEX TERMS:* 6218 Planetology: Solar System Objects: Jovian satellites; 5719 Planetology: Fluid Planets: Interactions with particles and fields; 6028 Planetology: Comets and Small Bodies: Ionospheres—structure and dynamics; *KEYWORDS:* Jupiter, Io, magnetic field perturbation, internal field, Hall effect, Alfvén wings

Citation: Saur, J., F. M. Neubauer, D. F. Strobel, and M. E. Summers, Interpretation of Galileo's Io plasma and field observations: I0, I24, and I27 flybys and close polar passes, *J. Geophys. Res.*, *107*(A12), 1422, doi:10.1029/2001JA005067, 2002.

1. Introduction

[2] The Galileo spacecraft in orbit around Jupiter since December 1995 performed several very interesting close flybys of the Galilean satellite Io. These flybys provided an excellent opportunity to study the flow of a sub-Alfvénic plasma past a body with a tenuous atmosphere. The first flyby in the wake of Io in December 1995, I0, yielded measurements of a surprisingly strong perturbed magnetic field [*Kivelson et al.*, 1996a, 1996b], strongly enhanced plasma densities and reduced plasma flows [*Frank et al.*, 1996; *Gurnett et al.*, 1996], and also a flux of directional high-energy electrons [*Williams et al.*, 1996, 1999; *Frank and Paterson*, 1999]. From the magnetic field measurements *Kivelson et al.* [1996a, 1996b] and *Khurana et al.* [1997] concluded an internal magnetic field at Io was required to explain the magnitude of the observed perturbation. This interpretation was later questioned by a series of authors, for example, *Frank et al.* [1996], *Neubauer* [1998a, 1998b], and *Saur et al.* [1999]. Two further flybys I24 and I27 provided measurements on a trajectory passing from the upstream side to the downstream side on the anti-Jovian facing side of Io [*Kivelson et al.*, 2001]. The I25 flyby below the south pole of Io yielded, unfortunately, only plasma wave observations and no plasma and magnetic field data. This polar pass might have produced definite conclusions on the nature of Io's magnetic field environment, which now might come from additional polar flybys I31 (August 6, 2001), I32 (October 16, 2001) and I33 (January 17, 2002).

[1]Now at Department of Earth and Planetary Sciences, Johns Hopkins University, Baltimore, Maryland, USA.

0148-0227/02/2001JA005067

[3] There have been several theoretical and numerical attempts to study Io's interaction with its plasma torus that have been reviewed, e.g., by *Neubauer* [1998a]. Recently, *Linker et al.* [1998] and *Combi et al.* [1998] applied a one-fluid magneto-hydrodynamic (MHD) model to simulate the I0 Io flyby in 1995. Both groups were able to model most of the overall amplitude of the observed magnetic field perturbation, but could not describe details of the field measurements such as its doubled peak structure. The advantages and disadvantages of these models in comparison to our model have been discussed in detail by *Saur et al.* [1999]. We would like to emphasize that to understand Io's plasma interaction it is essential to understand Io's electric current system which is controlled by an anisotropic conductivity distribution. *Linker et al.* [1998] used an inhomogeneous, but prescribed, isotropic ionospheric conductivity with additional pick up processes. *Combi et al.* [1998] used an ideal MHD model, with zero resistivity, i.e., infinite conductivity everywhere. Very recently, *Kabin et al.* [2001] modeled Io's interaction with a new description of mass loading at Io, which we will critique in a subsequent paper.

[4] In this paper we use an improved version of the plasma model presented by *Saur et al.* [1999] to reproduce the plasma and field measurements of the I0, I24 and I27 flybys and give predictions for a generic polar pass that will be applicable to the polar flybys I31, I32 and I33. Our model calculates, self-consistently, the densities, velocities and temperatures of the electrons and one ion species plus the electric field. This approach allows us to include self-consistently calculated anisotropic conductivities and pickup, recombination, heating and cooling rates. Although this model does not self-consistently calculate the magnetic field, we can use it to estimate from our three-dimensional electric current distribution the expected magnetic field perturbation by using Biot-Savart's law. We use these flybys to give a physical interpretation of Io's plasma interaction with its torus. It also allows us to address Io's internal magnetic field issue. We study the effects of different neutral atmospheres, and predict properties of the Alfvén wings when the Hall effect in Io's atmosphere is included.

[5] This paper is organized in the following way. In the next section we present our improved plasma model. Then we present the results of our model important for the general understanding of Io's interaction and then discuss the details about each flyby. We end with a summary.

2. Brief Model Description

[6] The foundation of this study is the model presented by *Saur et al.* [1999], which is a three dimensional two-fluid plasma model for electrons and ions. This model has undergone significant improvements and modifications which we will describe briefly in this section.

[7] We use the following Io-centric coordinate system, which is adjusted to the symmetries of the interaction and which thus depends on the actual system III position of Io in the torus. Our z axis is in the opposite direction to the local Jovian background magnetic field, the y axis is perpendicular to the plane given by the magnetic field and the orbital direction of Io. Thus the y direction is pointing roughly to Jupiter. The x axis completes the right-handed coordinate system and is consequently roughly in direction of the magnetospheric plasma flow. In our model we assume that the Jovian background field and the unperturbed plasma flow are perpendicular. This is not strictly true, and thus there is an ambiguity when we compare our model to the actual observations. Our coordinate system was chosen so that the actual Jovian magnetic field and the corotational electric field are identical with our background magnetic and electric fields. Please note, this coordinate system is similar to, but not identical with, the "IphiB"-system used by *Kivelson et al.* [2001], where their choice was to use the orbital direction of the satellite as identical with a coordinate axis (their x axis). Thus their z axis is not completely aligned with the background field, but is in the plane given by the orbital direction of the satellite and the background magnetic field.

2.1. Atmosphere Models

[8] In this study we apply three different atmosphere models. (a) First we use a radially symmetric model, to understand its basic impact on the plasma physics of the interaction. (b) Then we apply a modified neutral atmosphere to account for the very recent UV observations of Lyman-alpha emission from Io's poles, which *Roesler et al.* [1999] suggested and subsequently *Feldman et al.* [2000] concluded is evidence for a strong latitudinal dependence of Io's atmospheric SO_2 column density. Only a thin atmosphere is present at Io's polar caps which allows solar Lyman-alpha radiation to be reflected by the surface. Around Io's equatorial region, a dense atmosphere is present, which absorbs solar Lyman alpha radiation. These observations were then used by *Strobel and Wolven* [2001] to derive a latitudinal dependence of SO_2, which we adopt in this paper, i.e.,

$$n_s = n_{\text{pole}} + n_{\text{equator}} \exp\left[-(\vartheta/0.625)^6\right] \tag{1}$$

with the surface SO_2 density n_s, the latitude ϑ in radians, a background density $n_{\text{pole}} = 3.7 \times 10^{13}\ \text{m}^{-3}$ and an additional density enhancement $n_{\text{equator}} = 2.2 \times 10^{15}\ \text{m}^{-3}$ at the equator to be consistent with the HST observations. Note that the observations require a strong density decrease poleward of 30°. For our model a scale height of $H_0 = 80$ km is assumed, which gives an equatorial column density $N_n = 1.7 \times 10^{20}\ \text{m}^{-2}$. (c) Finally we use an atmosphere model with a longitudinal dependence. To determine this longitudinal dependence, we first look at the neutral atmosphere velocity equation

$$\rho_n \frac{d\mathbf{v_n}}{dt} = -\nabla p + \rho_n \mathbf{g} - \rho_n \nu_{ni}(\mathbf{v_n} - \mathbf{v_i}) \tag{2}$$

with ρ_n the neutral mass density, $\mathbf{v_n}$ the neutral velocity, $\mathbf{v_i}$ the ion velocity, ∇p the pressure gradient, $\mathbf{g}$ the gravitational acceleration of Io, ν_{ni} the neutral-ion collision frequency, and m_i and m_n the ion and the neutral mass, respectively. The radial force balance in most atmospheres, e.g., like the Earth, is hydrostatic balance of gravity and pressure gradient, which then determines the atmospheric scale height. When we look at Io and estimate the ratio of the ion drag force due to the plasma flow past Io's atmosphere (described by the last term in (2)) to the gravity force, we find that, assuming $v_n \ll v_i$,

$$\frac{\rho_n \nu_{ni} v_i}{\rho_n g} = \frac{n_i \langle \sigma v_i \rangle v_i}{g} \approx 1 \tag{3}$$

Table 1. Atmosphere Model

Parameter	(1) Standard	(2) Longitudinally Symmetric	(3) Radially Symmetric
H	80 km	80 km	80 km
θ variation	*Strobel and Wolven* [2001]	*Strobel and Wolven* [2001]	none
ϕ variation	$H(\phi) = H\,(1 + h_\phi \cos\phi)$; $n_{surface} = n_0\,(1 + h_\phi \cos_\phi)$; $h_\phi = 1/3$	none	none
n_0	2.2×10^{15} m^{-3}	2.2×10^{15} m^{-3}	2.2×10^{15} m^{-3}

with g = 1.8 m s^{-2}, a typical collision rate of atomic ions or SO_2^+ with SO_2 of $\langle \sigma v_i \rangle = 1 \times 10^{-14}$ m^3 s^{-1} with charge exchange included, and unperturbed torus properties n_i = 3.6×10^9 m^{-3}, v_i = 56 km s^{-1}. Note this ratio is also approximately correct in regions deep in Io's atmosphere where the density is enhanced by a factor of ten but at the same time the velocity is decreased by a factor of ten. We see that the drag force is of the same order of magnitude as the gravitational acceleration. On the upstream side where the drag force is in the direction of gravity, this results in an increased effective gravitational acceleration, and thus the actual scale height will be noticeably reduced. On the downstream side the effective gravitational acceleration is reduced by the drag force and thus we expect an enhancement in the scale height. To include this effect we used the following model for the neutral scale height dependence on longitude ϕ:

$$H(\phi) = H\big(1 + h_\phi \cos\phi\big) \tag{4}$$

with ϕ = 0 on the downstream side. We choose $h_\phi = 1/3$, so that there is a factor of two difference in scale height of the upstream to the downstream side.

[9] We expect that this drag force will induce a flow of neutral atmosphere from the upstream to the downstream side, which might result in a density enhancement on the downstream side. To include this effect we modify our model atmosphere surface density with the same dependence as the scale height given in (4). This is a simple way to implement the effect on the general structure of Io's atmosphere, although we believe that the actual density at Io's surface is determined by other processes. Equation (2) shows that a stationary solution must involve the full treatment of the velocity field $\mathbf{v_n}$ which is outside the scope of this work. In addition, we would like to note that there are also other plasma physical effects such as Joule heating that act on Io's atmosphere. A further discussion is however outside the scope of this paper. We summarize our three different atmosphere models in Table 1.

2.2. Improved Electron Temperature Description

[10] In our current model we also improve our electron temperature description by relaxing our assumption of an infinite electron heat conductivity everywhere along a field line. However, for numerical simplicity we do not solve the full electron temperature equation along each field lines. The principal idea of our description is that on the one hand in Io's ionosphere the electrons are strongly cooled due to a series of inelastic collisions, such as impact ionization, dissociation etc. On the other hand the Io plasma torus provides an extensive, but nevertheless limited, energy reservoir for the ionospheric electrons. However, the heat conduction from the torus into the ionosphere is not instantaneous but controlled by a limited heat flux. To model this effect we introduce two different spatial regions for each field line, with constant temperature within each region. One is the Io plasma torus with temperature T_e^{Torus} and the other is Io's ionosphere with T_e^{iono}. We solve for each temperature separately and at the boundary of both regimes we parameterize the heat flux by the local average of the heat conductivity in Io's ionosphere. The explicit equations are given in the appendix.

2.3. Field-Aligned Energetic Electrons as Ionization Source

[11] In the model of *Saur et al.* [1999], we considered the ionization sources electron impact ionization by the thermal electron population, and photoionization. Now we add a third ionization source, based on the high-energy bidirectional electrons observed by *Williams et al.* [1996, 1999] and *Frank and Peterson* [1999]. *Williams et al.* [1996, 1999] basically measured a power law distribution of the bidirectional electron flux in the range of 22 keV up to about 150 keV. We fit a power law to the particle flux measurements of *Williams et al.* [1999], convert it to phase space density, and then compute the ionization rate of SO_2 using its energy dependent ionization cross-section. The free parameter in this high-energy electron ionization rate is the lower energy limit for extrapolation of the power law. We adopted ~2 keV for this limit to obtain an energy flux of 3×10^{-3} J m^{-2} s^{-1} (= 3 erg cm^{-2} s^{-1}) which is consistent with *Frank and Peterson* [2000] and gives an ionization rate of about 8 times the photoionization rate for zero optical depth. In the absence of a generally accepted theory for the formation of the bidirectional electrons, we have to make some arbitrary assumptions for their spatial distribution. We note that *Thorne et al.* [1999] present an explanation for the evolution of the electron distribution outside the wake region where the bidirectional electrons are observed. We assume that field-aligned electrons form with Io's evolving interaction from the upstream to the downstream side, and thus exist mainly on the downstream side, and additionally that they are absorbed in flux tubes that intersect with Io. We use the following expression for the spatial distribution of the ionization rate due to the bidirectional electrons

$$f_{\text{williams}} = f_{\text{williams},0} \exp\left[-\left(R_{\text{Io}} - \sqrt{x^2+y^2}\right)/H_{\text{williams}}\right] \cdot \left(\frac{x - x_{\text{up}}}{\sqrt{x^2+y^2}}\right)^2 \text{Geo}(x,y) \tag{5}$$

with

$$\text{Geo} = \begin{cases} 0 & \text{for} \quad x < x_{\text{up}} = 3/5 R_{\text{Io}} \\ 0 & \text{for} \quad (x^2+y^2)^{1/2} < R_{\text{Io}} \\ 0 & \text{for} \quad (x^2+y^2)^{1/2} > 2.4 R_{\text{Io}} \\ 1 & \text{for} \quad \text{all other points} \end{cases} \tag{6}$$

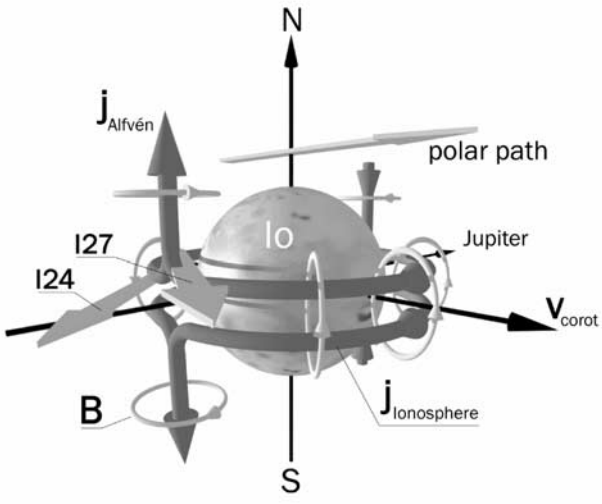

Figure 1. Sketch of electric current system and its associated magnetic field at Io. The current system consists of the ionospheric currents mainly in the direction from the Jupiter facing side to the side opposite of Jupiter, and the Alfvén wing currents roughly in the same direction as the background magnetic field. Circles around the sketched electric current indicate its generated magnetic field.

with a scale $H_{\text{williams}} = R_{\text{Io}}/2$, and a geometry factor that sets this electron flux to zero on upstream flux tubes $x - x_{\text{up}} < 0$ (x_{up} = 3/5 R_{Io}), on magnetic field lines through Io, and at larger distance, i.e., outside of Io's atmosphere (in rough accordance with *Williams et al.* [1996, 1996]). The term in parenthesis before Geo varies for $x_{\text{up}} = 0$ as the cosine of the longitude squared, but allows for $x_{\text{up}} > 0$ for some ionization toward the upstream side. Note that the energetic electrons are important in this model only as an ionization source and thus the actual distribution outside of Io's atmosphere is therefore of no concern for our purposes.

2.4. Io's Electric Current System and Magnetic Field

[12] The heart of Io's electrodynamic interaction is its electric current system, which we sketch in Figure 1. This current system controls the plasma flow around Io, creates a prominent magnetic field signature and forms Io's Alfvén wings. The current system is enabled by the anisotropic ionospheric conductances with a dominant contribution from atmospheric collisions and a smaller contribution due to pickup (see *Neubauer* [1998a] and *Saur et al.* [1999] for further details). It is driven by the corotational electric field in the rest frame of Io whose ultimate source is the flow of magnetized torus plasma past Io and its atmosphere. When we look at the main force balance in Io's ionosphere, we note that the ion neutral collisions and the pickup processes determine the force to slow down the plasma. They drive at the same time the ionospheric electric currents which in turn establishes the force balance to reaccelerate the plasma by the j × B force. In our model we calculate both the main electric currents (see discussion directly below) and the plasma flow self-consistently.

[13] The electric current system can be decomposed into field-aligned and perpendicular electric currents. In the ionosphere most of the perpendicular currents are the ohmic Pedersen and Hall currents, flowing mainly from the Jupiter facing side of Io to the anti-Jupiter side. These currents then continue along the magnetic field lines out of the ionosphere and then finally feed into the Alfvén wing currents. The Alfvén wing currents enter Io's ionosphere on the side facing toward Jupiter and leave Io's ionosphere on the opposite side. This situation is similar both on the northern and southern hemisphere. This system carries an electric current of about 10 Million A through Io's ionosphere or 5 Million A through each hemisphere [*Saur et al.*, 1999].

[14] In addition to the ionospheric Ohm's current, i.e., the Pedersen and Hall currents, there are contributions from diamagnetic and inertia currents [see, e.g., *Baumjohann and Treumann*, 1996, chap. 7.4]. We propose that these currents are responsible for the unexplained double-peak structure in Io's magnetic field observations obtained during the December 1995 flyby. Whereas we calculate the Ohm's current self-consistently within the framework of our model, we estimate the diamagnetic currents by

$$\mathbf{j}_{\text{dia}} = -\frac{\nabla p \times \mathbf{B}_0}{B_0^2} \tag{7}$$

and the inertia currents by

$$\mathbf{j}_{\text{inert}} = -m_i n_i \frac{\mathbf{v_i} \cdot \nabla \mathbf{v_i} \times \mathbf{B}_0}{B_0^2} \tag{8}$$

without consideration of the action of the plasma pressure and plasma inertia (in the ionosphere) on the plasma velocity and the electric field. (Note that in the Alfvén wing solution of *Neubauer* [1980] the plasma inertia is self-consistently included.) Here, $\mathbf{B_0}$ is the Jovian background magnetic field at the location of Io, p the plasma pressure, $\mathbf{v_i}$ the ion velocity, m_i the ion mass, and n_i the ion density. The diamagnetic and the inertia currents are overall small compared to the Ohm's current (see section 3.2). We neglect to first order their action on the electric field and the plasma flow, which are mostly dominated by the ion-neutral collisions and pickup. We can use this electric current system to calculate a first order magnetic field perturbation using Biot-Savart's law.

3. Results

[15] In this section we will describe the results of our numerical model. Our strategy here is to focus mainly on the case that has the most realistic atmosphere, i.e., with a longitudinal and latitudinal dependence. This is the standard atmosphere model described in section 2.1. We will show, in addition, results of other runs to emphasize how different atmosphere models or different input parameters affect the model results and thus give insight into their physical role for Io's interaction. In Table 2 we give the plasma values and numerical parameters used in our model runs and in Table 1 we summarize the atmospheric models.

3.1. General Considerations

[16] Before we compare observable quantities with our modeled results, we first discuss general results which are

Table 2. Model Plasma Parameters

Parameter	Value
Numerical Resolution	$R_{Io}/100$
Magnetic field B_0	1.835×10^{-6} T
plasma velocity v_0, relative to Io	45 km s^{-1}
Alfvén conductance Σ_A	5.1 S
Upstream electron density $n_{e,0}$	3.6×10^9 m^{-3}
Upstream electron temperature $T_{e,0}$	5 eV
Extension of plasma torus R_{Torus}	7×10^7 m

We have used uniform resolution over a Cartesian grid with size 4.8 R_{Io} $\times$ 4.8 R_{Io} $\times$ 2.4 R_{Io} for the plasma fluid quantities. The electric field is calculated on a grid 20 R_{Io} $\times$ 20 R_{Io}. Note that the extension of the torus enters in (A4) as $R_u = R_{Torus}$. For more details about the numerics, see also *Saur et al.* [1999].

important to understanding the observations along each trajectory.

3.1.1. Electric Potential and Conductances

[17] We start with a discussion of Io's conductances, electric field environment, and electron streamlines, which are crucial for the formation of Io's ionosphere. The ionosphere of Io is convection dominated and is not in static chemical equilibrium as will be apparent in the density and temperature profiles.

[18] In Figure 2 we show the electric potential and in Figure 3 we display Io's Pedersen conductivity. The Hall conductance is qualitatively similar and thus not displayed. The Pedersen conductivity strongly reflects the neutral

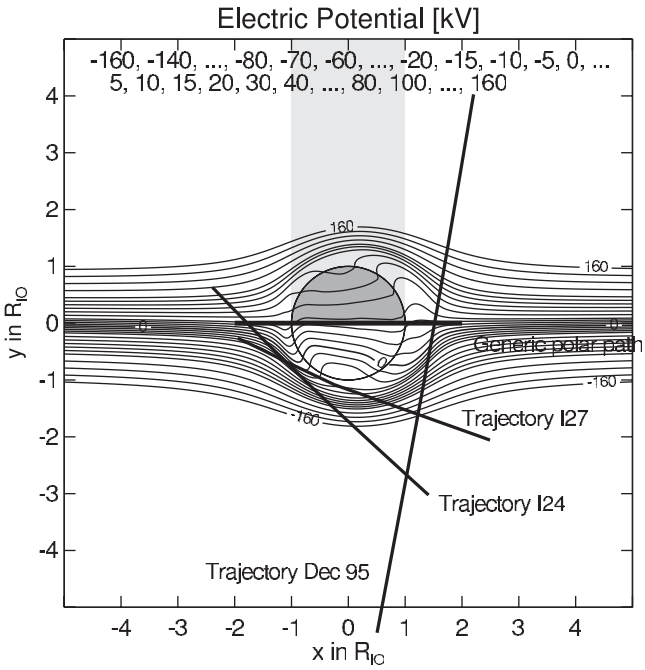

Figure 2. Electric potential at Io. Isolines are trajectories of the electrons. Outside Io's ionosphere, the isolines are also trajectories of the ions. Additionally, the flyby trajectories of the Galileo spacecraft projected into Io's equatorial plane are shown. Note that the electric potential is a two-dimensional quantity which is independent of z (along the magnetic field lines). The displayed streamlines that intersect with Io are actually only possible when the plasma passes above or below Io. We display Io and its shadow only for facilitation of the reader's orientation.

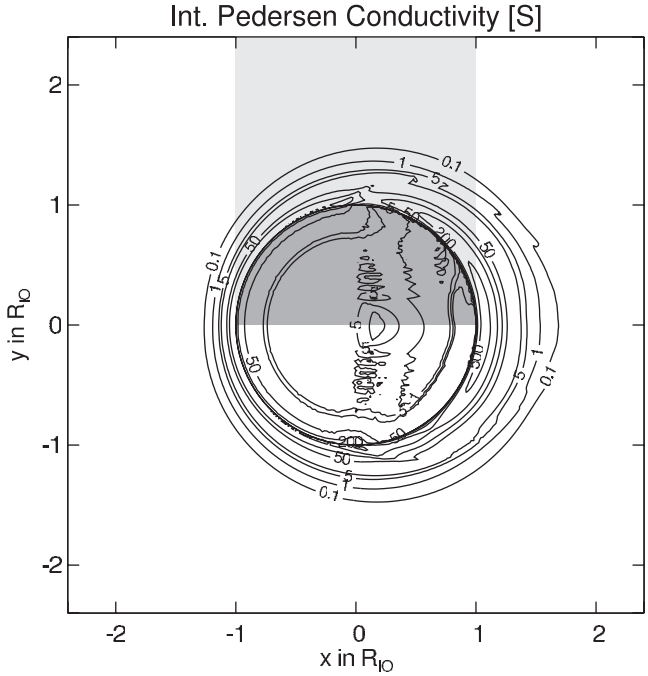

Figure 3. Integrated Pedersen Conductances Σ_1 in S for standard model. Note that Σ_1 is a two dimensional quantity. We display Io and its shadow only for facilitation of the reader's orientation.

atmosphere model. (a) The latitudinally dependent neutral atmosphere has very little density above the poles and thus the integrated conductivity is very small there. It maximizes in an annulus around Io due to high equatorial density and the long path length for calculating the integrated conductances. The Pedersen conductance reaches maximum values of more than 500 S. We note that these values are higher than the conductances in the Earth ionosphere since the magnetic field at the Earth is about factor of 25 higher. For the same reason the conductances in Jupiter's ionosphere are very small. (b) The scale height for the conductance on the upstream side is clearly smaller than on the downstream side due to the longitudinal dependence of the neutral atmosphere. The Pedersen and Hall conductances determine the electric field, or the electric potential, shown in Figure 2. Isolines of the electric potential are streamlines of the electron flow. Figure 2 shows that Io's electron flow is strongly directed around Io and slowed near Io. Because the conductance is small across the pole the action of the Hall effect is also small in this region and the electron flow is only strongly rotated toward Jupiter where the Hall conductance is high, i.e., in an annulus around Io.

3.1.2. Electron Density

[19] In Figure 4, we show Io's equatorial electron density. The electron density increases mostly from the upstream to the downstream side. The high-energy electrons [*Williams et al.*, 1996, 1999; *Frank and Peterson*, 2000] that we include as an energy source in addition to electron impact ionization of the thermal electrons and photoionization suffice to create an extensive ionosphere in Io's wake. In the simulations shown by *Saur et al.* [1999] we had a nearly empty wake because the electrons convecting from the upstream side are absorbed by Io and the model had no sufficient ionization

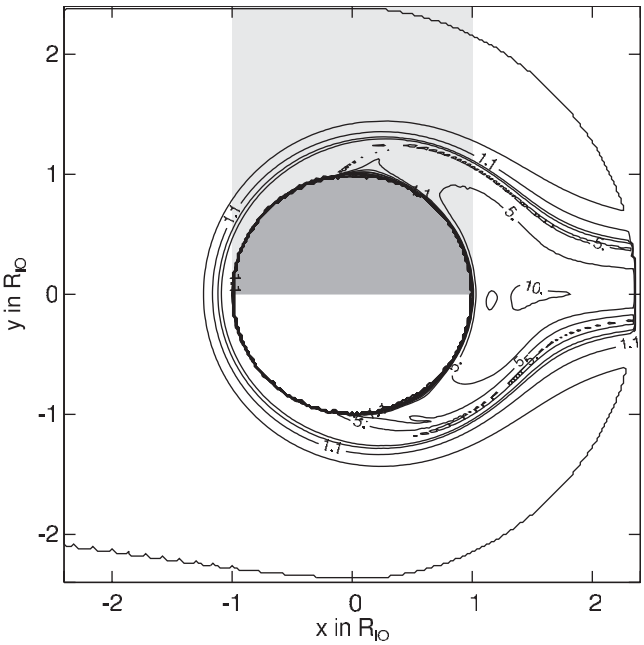

Figure 4. Electron density in upstream values $n_{e,0}$ in the equatorial plane for standard model.

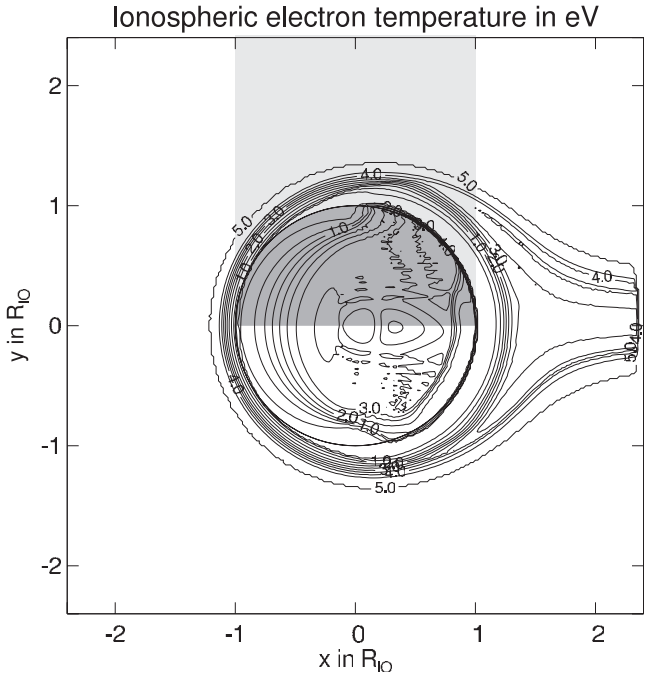

Figure 5. Electron temperature in eV in Io's ionosphere for standard model. Note that the ionospheric electron temperature is a two-dimensional quantity in our model. We display Io and its shadow only for facilitation of the reader's orientation.

source in the wake. We do not solve for the velocity equation parallel to the field lines and thus no plasma from above the poles can flow into Io's wake. As we will see when we discuss the I0 flyby of 1995 the ionization of the high-energy electrons contribute significantly to the observed plasma density in Io's wake.

[20] Our modeled electron density is also in general agreement with the radio-occultation measurements of *Kliore et al.* [1975] and *Hinson et al.* [1998], however we are not able to reproduce their high surface electron densities. According to *Strobel et al.* [1994], Io's atmosphere has a small atmospheric scale height with a high neutral atmosphere density near the surface, which we cannot resolve with our numerical model. A high neutral density might slow the plasma flow close to Io's surface more, which would then allow higher ionospheric densities to be built up. In addition, consideration of multi ion-chemistry including atomic ions might also enhance our modeled electron density. (See also section 3.4.)

3.1.3. Electron Temperature

[21] In Figures 5 and 6 we show our modeled ionospheric and torus electron temperature. The upstream torus electron fluid has a temperature of 5 eV. Due to inelastic collisions with the neutral atmosphere the ionospheric temperature is decreased. It is most strongly reduced (to less than 1 eV) where the neutral atmosphere is the most dense. In addition, in this region electron heat conduction that enables energy flow from the torus into the ionosphere is least efficient. The electrons in the torus lose energy due to this heat flux into Io's ionosphere. Because there is no energy source in the torus the electron temperature steadily decreases as flux tubes move across Io. The heat flux is very anisotropic and thus occurs in our model only parallel, and not perpendicular, to the field lines. Therefore the electron density profile strongly reflects the anisotropic nature of Io's interaction, which is controlled by the strong background magnetic field

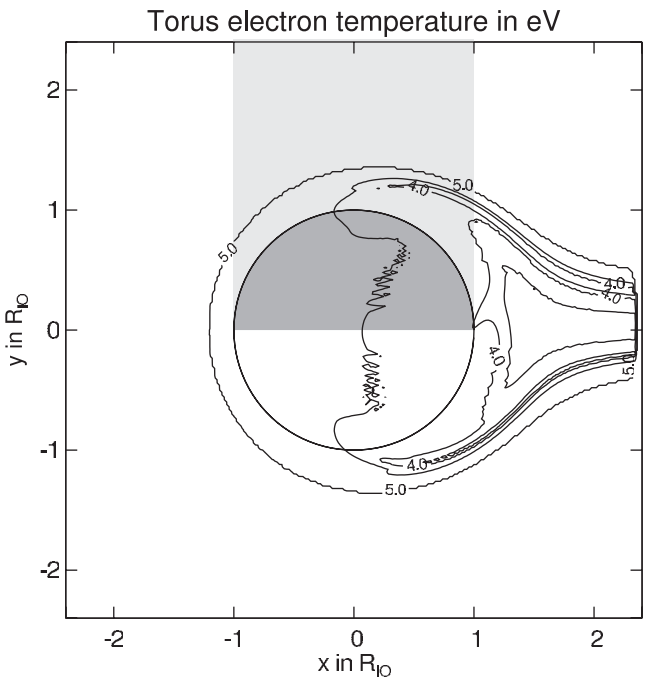

Figure 6. Electron temperature in eV in plasma torus for standard model. Please note that the torus electron temperature is a two-dimensional quantity in our model. We display Io and its shadow only for facilitation of the reader's orientation.

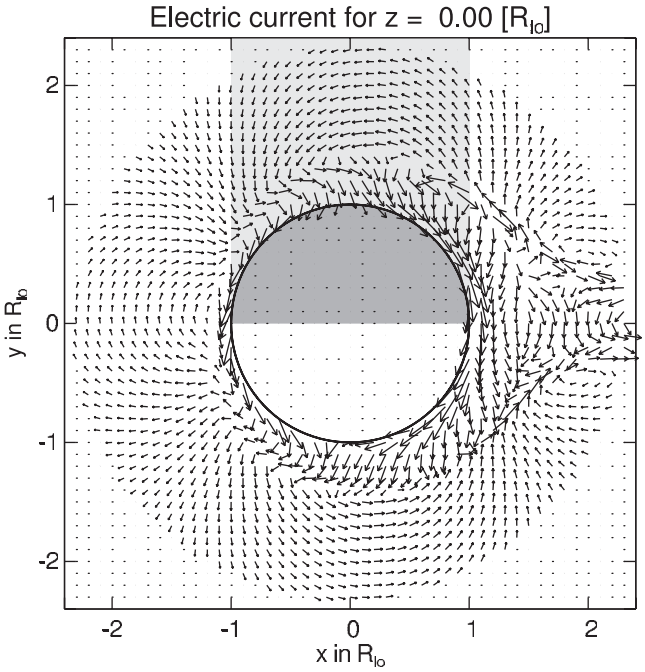

Figure 7. Electric current in the equatorial plane for standard model. For clarity reasons, the length of the vectors are displayed so that a difference of a factor of ten in magnitude is actually displayed as a factor of two.

of Jupiter at the location of Io. This explains the morphology of Io's auroral UV emission observed by *Roesler et al.* [1999], which strongly depends on the electron temperature and thus consequently on the local background magnetic field [*Saur et al.*, 2000]. In the polar regions of the ionosphere the electron temperature is increased again because the neutral atmosphere density is small. Thus here sinks are small and at the same time heat conduction from the torus into the ionosphere is very efficient. Similarly downstream of Io's atmosphere, i.e., in the wake, both temperatures equalize again.

3.1.4. Electric Current System

[22] Now we describe our modeled electric current system which is important for understanding Io's magnetic field environment. The principal structure of the current system is shown in Figure 1. We show the numerically modeled equatorial electric current in Figure 7 and the current in the plane given by $x = 0$ in Figure 8. The $x = 0$ plane is the plane through Io's center and perpendicular to the unperturbed plasma flow, i.e., including the z axis along the background magnetic field and the y axis roughly toward Jupiter. In Figure 8, one can see the parallel electric current coming down from Io's northern and southern Alfvén wings on the side facing Jupiter. In the dense part of Io's atmosphere the ionospheric conductivity is high and thus current can flow perpendicular to the magnetic field lines. This can be seen in Io's equatorial region. Because the body of Io is an insulator the current is continued around Io both in the equatorial region (Figure 7) and across the pole (Figure 8). The general direction of the ionospheric current is mainly from the side facing Jupiter to the opposite side. Since we have a small neutral polar density and thus small conductivity in this model, not all the electric current can be continued across Io's pole and is thus partly continued above the pole as parallel electric current out of Io's ionosphere.

[23] In Figure 7 the equatorial current system consists of the ionospheric Pedersen and Hall currents close to the surface. Further away from Io are the inertia currents that come from the slowing and redirecting of the plasma flow around Io. In the wake of Io the diamagnetic current due to the plasma pressure gradient plays an important role. The plasma in the wake is cold since it is picked up close to Io where the plasma velocity is low. Thus there is a pressure gradient from the center of the wake to its boundaries which points away from the Io plasma wake. This drives an electric current away from Io on the Jupiter facing side of the wake boundary and an electric current toward Io along the wake boundary on the anti-Jupiter side of Io (see Figure 12). The closing of the plasma flow on the downstream side of Io also produces inertia currents in the general direction of the diamagnetic currents. However, this picture is further complicated in our model due to the more complicated wake pressure structure that results from the inhomogeneous wake plasma density distribution.

[24] Further away from Io (ca 1/3 R_{Io}), the inertia currents are also clearly visible, they have the large scale form of a four leaf clover, with one leaf on the upstream side, another on the downstream side, and one on each flank. This form represents the large scale velocity field of the plasma flow which is decelerated on the upstream side, directed around Io and reaccelerated in the wake. This same principal form of the inertia currents also applies to Io's Alfvén wings

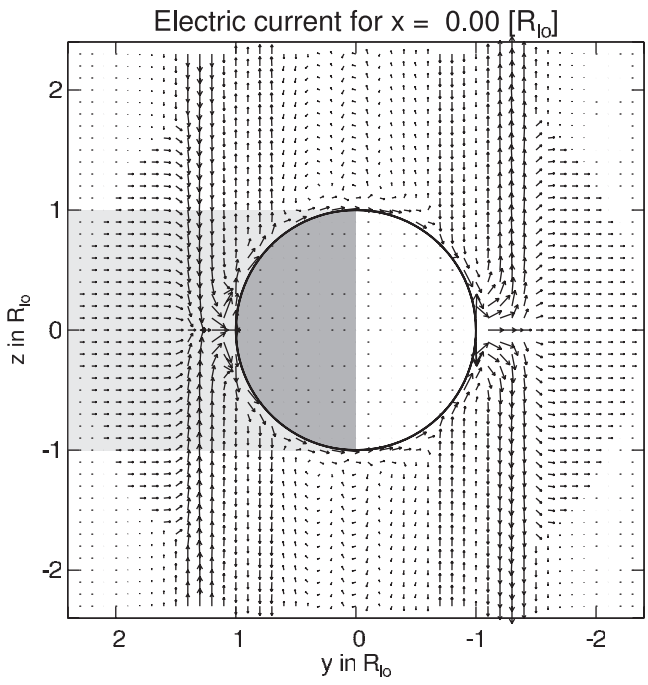

Figure 8. Electric current in the plane x = 0, i.e. parallel to background magnetic field, for standard model. For clarity reasons, the length of the vectors are displayed so that a difference of a factor of ten in magnitude is actually displayed as a factor of two.

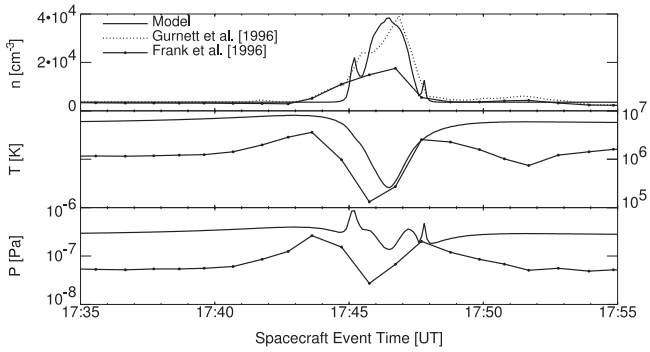

Figure 9. Plasma density, ion temperature and pressure for the I0 flyby for standard model and observed data by *Frank et al.* [1996] and *Gurnett et al.* [1996].

where the plasma is slowed down and accelerated again downstream [see *Neubauer*, 1980]. Since this work focuses on the local interaction of Io, we have neglected for simplicity the inertia currents and diamagnetic currents outside of Io's ionosphere for our magnetic field estimates. Io's global electric current system as described above is essential for understanding Io's magnetic field environment.

3.2. I0 Flyby

[25] With the above context, we now examine the Galileo spacecraft flyby observations. The I0 flyby in December 1995 was on the downstream side and through Io's wake in the equatorial region as can be seen in Figure 2.

[26] In Figure 9 we show the plasma density, the ion temperature and the plasma pressure calculated along the I0 trajectory. Our plasma profile matches very well the actual observations of *Gurnett et al.* [1996]. The profile of *Frank et al.* [1996] has slightly smaller values, which are probably due to multiply charged ions. Since our model assumes a singly charged SO_2 fluid and an electron fluid, we consequently try to achieve agreement with the electron density measurements of *Gurnett et al.* [1996]. The high-energy electrons of *Williams et al.* [1996, 1999] and *Frank and Peterson* [2000] that we include in our model as a third ionization source fills our otherwise rather empty wake [see *Saur et al.*, 1999]. This ionization source acts as a "catalyst" to create secondary electrons and thus an enhanced thermal electron population that can tap the torus electron heat reservoir by heat conduction. Once there is a sufficient electron seed population, the thermal electrons are able to efficiently contribute to the ionization process. The two small side maxima in our model density come from the plasma that makes it along the flanks of Io's ionosphere and thus has a very long path length over which it becomes significantly mass loaded. Our model plasma temperature is a good description of the measured values only close to Io. As explained by *Saur et al.* [1999], for the ion temperature we use a simplified solution given by the local ion velocity. This is valid only very close to Io where the atmosphere is dense. However, our model ion temperature enters only weakly in the ion neutral collision frequency and thus further away from Io has no significant effect on other primary properties of our solution (i.e., the properties that we calculate self-consistently, see the discussion by *Saur et al.* [1999]). The plasma pressure then simply reflects our model density and temperature. However, we point out that we use the plasma pressure to calculate the diamagnetic currents and subsequently its contribution to the magnetic field perturbation. Although the simplifying assumption in our ion temperature description might introduce some uncertainties in the associated currents and calculated magnetic fields, the general effect that produces the double peak in the magnetic field structure discussed further below will not be affected.

[27] In Figure 10, we show our plasma velocity along with data by *Frank et al.* [1996]. The measurements and the model show a strongly reduced plasma flow (mostly apparent in the magnitude and the v_x component) and also how the flow is directed around Io (see the v_y component which has the direction of a flow that is first swept around and then closes behind Io).

[28] The magnetic field measurements of the I0 flyby [*Kivelson et al.*, 1996a, 1996b] are shown in Figure 11. In order to compare the data directly with the numerical output of our model we linearly detrended the actual observations. For the x, y, and z components this is equivalent to displaying the perturbations from an assumed locally linearly varying background magnetic field. This procedure holds for all figures which show observed data along with our model results. In addition, our modeled values which we display with the observations are rotated into the coordinate system in which the observational data or trajectory information are tabulated. This is for the I0 flyby the "iphi0"-system [*Kivelson et al.*, 1996a, 2001], where the x axis is in direction of Io's orbit, and the z axis aligned with Jupiter's spin axis. Results for I24 and I27 are compared in our model coordinate system defined in section 2.

[29] The magnetic field observations indicate a strongly perturbed magnetic field near Io which has given rise to different interpretations. As shown in Figure 11, the observed magnetic field perturbation has a peak value of about 1000 nT. In addition a prominent double-peak structure is also visible. In our model a total current of about 10 Million A flow through Io's ionosphere mostly on the upstream and the downstream sides. Using the right hand rule (see Figure 1), it can be seen that this current creates a

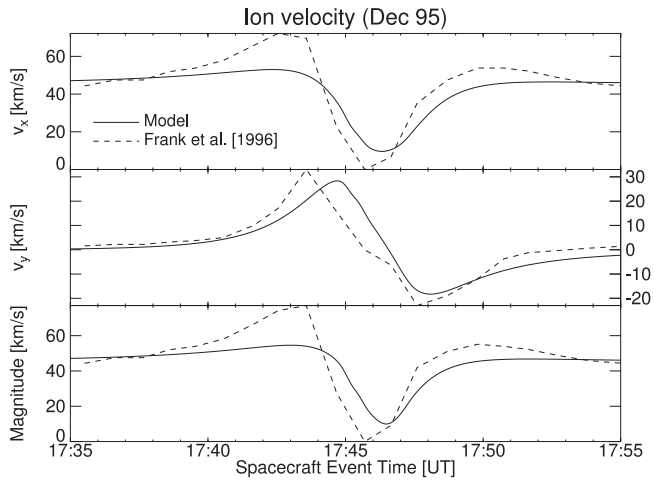

Figure 10. Ion velocity for the I0 flyby for standard model and observed data by *Frank et al.* [1996].

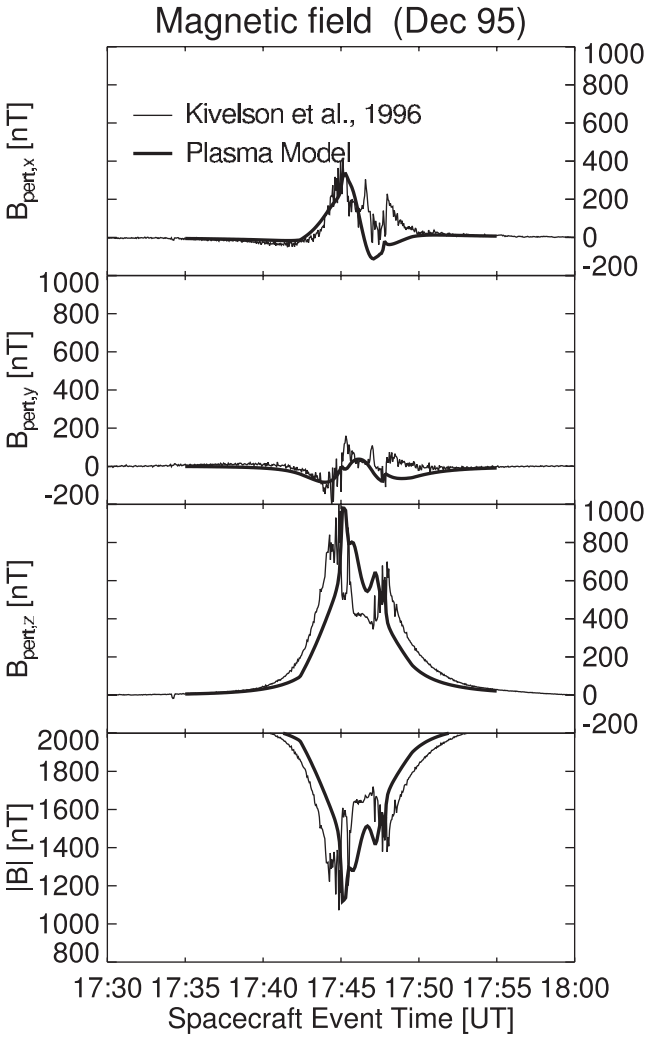

Figure 11. Magnetic field for I0 flyby for standard model.

magnetic field component in the opposite direction of the background magnetic field, as is shown in the third and fourth panel of Figure 11 for the z component (in opposite direction of the background field) and the magnitude, respectively. Our calculated magnetic field matches very well the observations without the assumption of an internal magnetic field, in contrast to the inference by *Kivelson et al.* [1996a, 1996b] and *Khurana et al.* [1997].

[30] We are also able to reproduce the observed double-peak structure. This is formed from the wake diamagnetic and the inertia currents which flow mostly on the flanks of the wake, and thus generate a magnetic signature in the center of the wake that is in the direction of the background field (see also section 2.4). As shown in the schematic Figure 12, this signature is in the opposite direction to the main perturbation signature produced by the ionospheric ohmic currents and thus produces the ''valley'' in the magnetic field signature at the center of the wake. We show the different contributions in our model fields in Figure 13. As can be seen in the third panel, the Ohm's electric currents (dashed line) have the dominant contribution to the model field. It can account for the observed strength of the magnetic field signature in the z direction. The diamagnetic currents (dotted line) and the inertia currents (thin solid line) are clearly smaller in magnitude, but they contribute to the generation of the observed double-peak structure.

[31] In the first panel of Figure 11, we show the x component of the magnetic field, which also fits the observations fairly well. Before 17:47 the Galileo spacecraft trajectory was located south of Io's magnetic equator. In the downstream region of the southern hemisphere, j_z, and also j_y contribute to a positive x component of the magnetic field, which then after 17:47 changes sign on the northern hemisphere. For the y component in the second panel of Figure 11 both our model and the observations show only a very small perturbation.

[32] Now we turn to the effect of an upstream and downstream asymmetry. It is interesting to compare the above results with the magnetic field of a model where we used a longitudinally symmetric atmosphere. This is displayed in Figure 14. The essential component for the internal field issue is the z component (panel 3), i.e., parallel to the background magnetic field. Our model B_z underestimates the observed field. One of the effects of an asymmetric atmosphere with larger scale height on the downstream side than on the upstream side is an asymmetric distribution of electric current with more electric current on the downstream side than on the upstream side. Therefore, with more than half of the total 10 Million A close to the flyby trajectory of I0, we can calculate the observed asymmetry of a maximum perturbation of about 300 nT on the upstream side (see section 3.3.2) and about 600 nT on the downstream side.

[33] We would like to comment on the uniqueness of our modeled results. So far our approach has been to use an

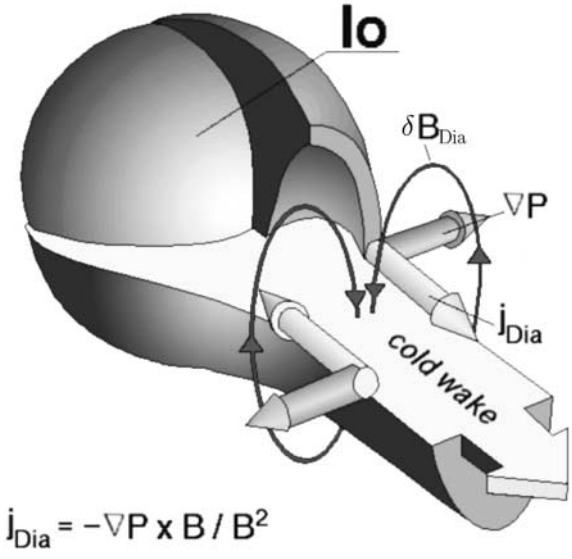

Figure 12. Sketch how the diamagnetic currents j_{Dia} produce a magnetic field perturbation δB_{Dia} and thus the ''valley'' in the overall magnetic field signature, which results in the observed double peak structure. The inertia of the plasma shielded around Io, which closes again in the wake, (i.e. $v_y \partial_y v_y$) has the same principal action on the magnetic field.

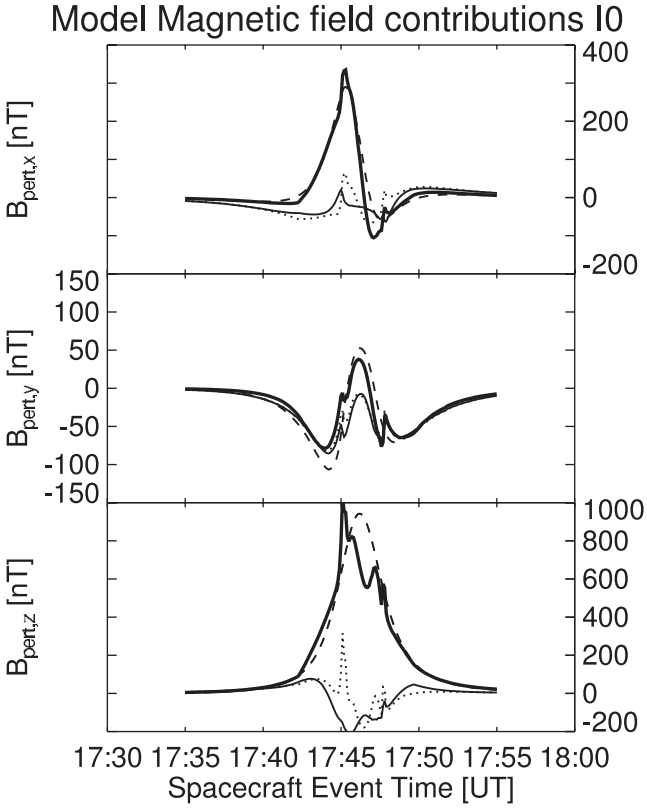

Figure 13. Magnetic field contribution for I0 flyby for standard model, fat solid line: total model field, dashed line: contribution from Ohm's current, dotted line: contribution from diamagnetic currents, thin solid line: contribution from inertia currents. We do not display the magnetic field magnitude because each contributor adds nonlinearly to the total magnitude.

atmosphere model which is constrained by remote sensing observations and which gives, at the same time, the best results when compared to the Galileo spacecraft measurements in the absence of an internal magnetic field. However, since there is no precise knowledge on the detailed structure of the neutral atmosphere, we could pose the question: Is it possible to explain the Galileo observations with an internal magnetic field of the strength inferred by *Kivelson et al.* [1996a, 1996b] and a very exotic neutral atmosphere? This would require a conducting path that directs most of the current to the upstream side and nearly none on the downstream side with an upstream perturbation of about 900 nT that compensates for the 600 nT of an internal field and yields the observed 300 nT in the negative direction. This seems to be rather implausible to us and in contradiction with the plasma observations of a larger plasma density on the downstream side than on the upstream side.

3.3. I24 Flyby

[34] The second close flyby I24 began on the upstream side of Io and then passed on the anti-Jovian side in direction downstream as sketched in Figure 2. The closest approach occurred at an altitude of about 600 km.

[35] The upstream plasma parameters that we used in all our models are the values measured during the I0 flyby and are given in Table 2 although the upstream conditions were different for I24 and I27. The underlying philosophy is that we (a) wish to keep the numerical output within limits and (b) to compare the effects of different neutral atmosphere models on the plasma physics at different locations of the interaction, i.e., for different flybys. Therefore we normalized, for I24 and I27, all the measured and modeled upstream torus values to unity.

3.3.1. Plasma Density and Velocity

[36] On the upstream side we expect a less developed plasma interaction than on the downstream side for several reasons. Io's interaction is strongly controlled by convection as discussed in section 3.1 and thus plasma densities generally increase from the upstream side toward the downstream side. This is evident in the plasma profile along the I24 pass (shown in Figure 15) where we calculate no density increase in agreement with a flat electron density profile reported by *Gurnett et al.* [2001], i.e., the Galileo spacecraft passed outside of Io's ionosphere. However, the measured ion density of *Frank and Paterson* [2000] shows variations along the I24 flyby. These differences may be due to the inferences of ion charge states and plasma velocities associated with the data analysis and cannot be evaluated by us. The flat signature is also evidence that there is no

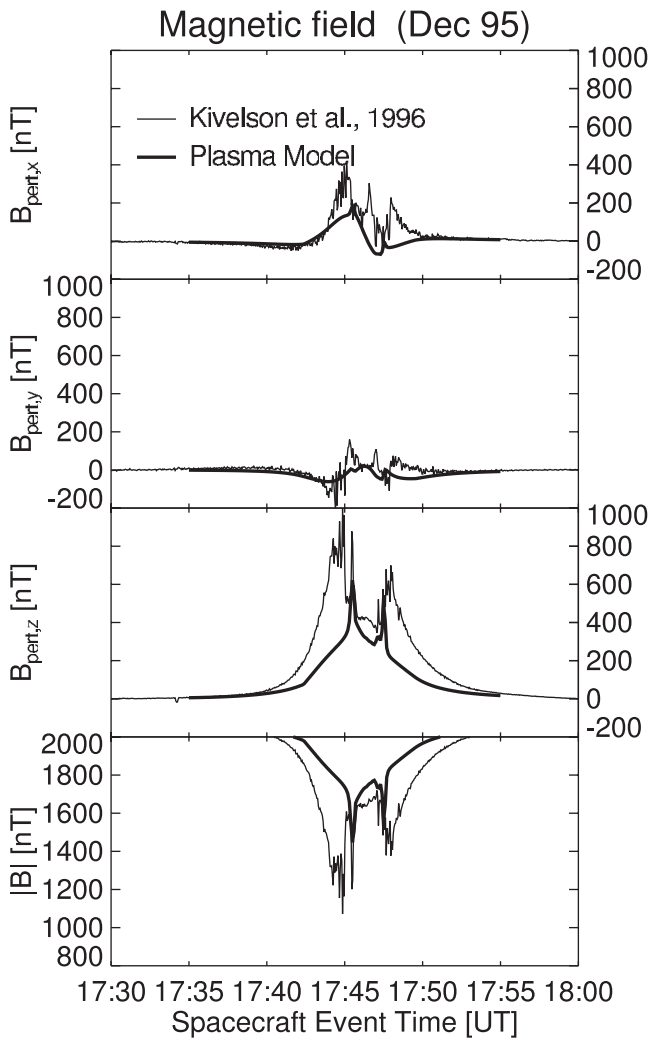

Figure 14. Magnetic field for I0 flyby for longitudinally symmetric atmosphere model.

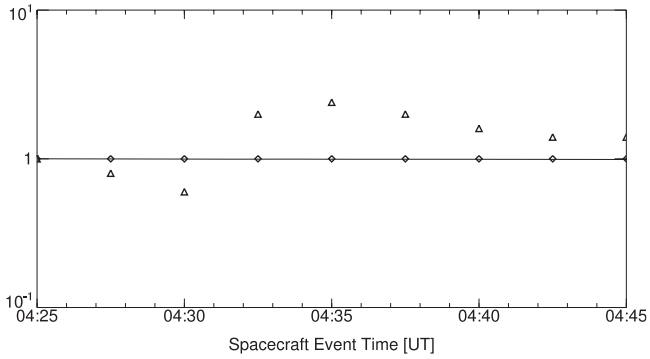

Figure 15. Modeled plasma density for I24 flyby for standard model (solid line) in $n_{e,0}$ (see Table 2) and observed data by *Gurnett et al.* [2001] (diamonds) and *Frank and Paterson* [2000] (triangles). Note observed values are also normalized to the measured upstream conditions, respectively.

significant neutral atmosphere density upstream of 600 km, which helps to constrain Io's neutral scale height. In this model we use a constant neutral atmosphere scale height in contrast to the model by *Saur et al.* [1999] (see equations (1) and (2) therein). We find that for H = 80 km, as well as for an asymmetric atmosphere with H = 53 km on the upstream side, no upstream density enhancement for I24. However, with our earlier neutral atmosphere model [*Saur et al.*, 1999] we would predict a modest plasma enhancement along the I24 trajectory.

[37] However, the ion velocity is noticeably perturbed as expected for flow diverted around Io (see Figure 16) and in agreement with the observations reported by *Frank and Paterson* [2000]. The plasma velocity is controlled by the electric field which reacts nonlocally to polarization charges produced by the electric current system. This behavior is as expected mathematically from the electric potential equation (described by *Neubauer* [1998a] and *Saur et al.* [1999]), which we use for calculating the electric field. It is an elliptic partial differential equation, characterized by nonlocal behavior. Thus the action of the electric current is evident already quite far upstream of Io with a plasma flow reduced on the upstream side and accelerated on the flanks of Io (in Figure 16 at times larger than 4:35 UT). This is the typical behavior expected for a two-dimensional dipole, by which Io's perturbation electric field can be described to first order.

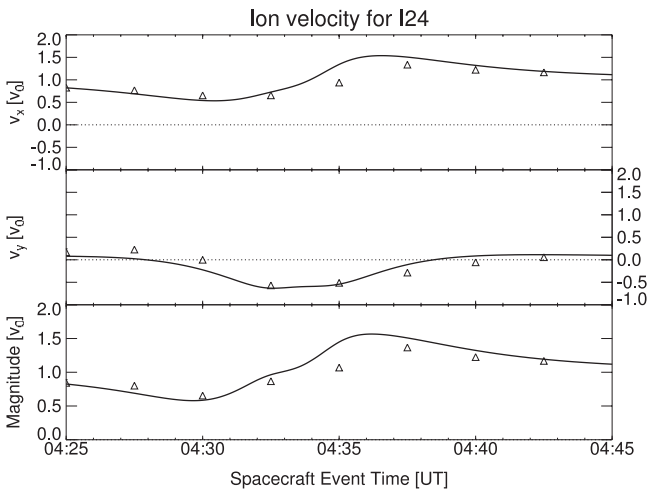

Figure 16. Normalized ion velocity for I24 flyby for standard model (solid line), and observed data by *Frank and Paterson* [2001] (triangles).

3.3.2. Magnetic Field

[38] In Figure 17 we show the magnetic field perturbation that we model along the I24 trajectory. Since the flyby was on the upstream side of Io, the effect of the ionospheric current system on the magnetic field is in the opposite direction to that on the downstream side. Thus the z component of the field points in the direction of the background magnetic field, and thus results in an increased magnetic field magnitude. An internal magnetic field would produce on the upstream side a signature in the same direction as on the downstream side of about the same magnitude (500 to 600 nT) at the same distance from the satellite. Since we do not see such a signature in the opposite direction this can be interpreted, albeit not uniquely, as evidence for at most a very weak internal field. We note that for the upstream I24 flyby we calculated the inertia currents with an average upstream torus ion mass of 20 amu instead of 64 amu for the ionospheric SO_2^+.

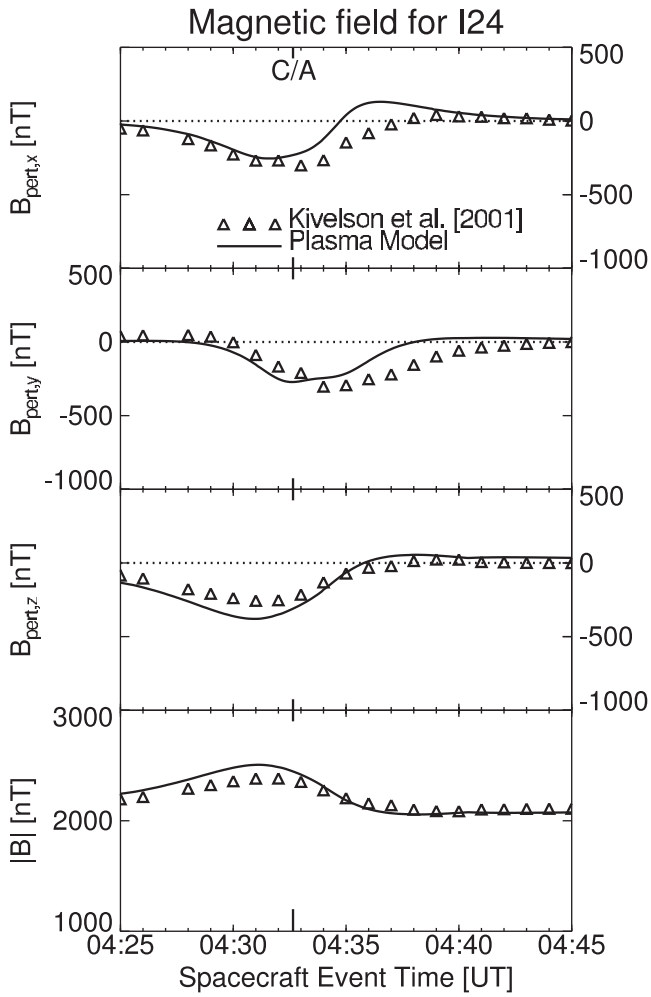

Figure 17. Magnetic field for I24 flyby for standard model.

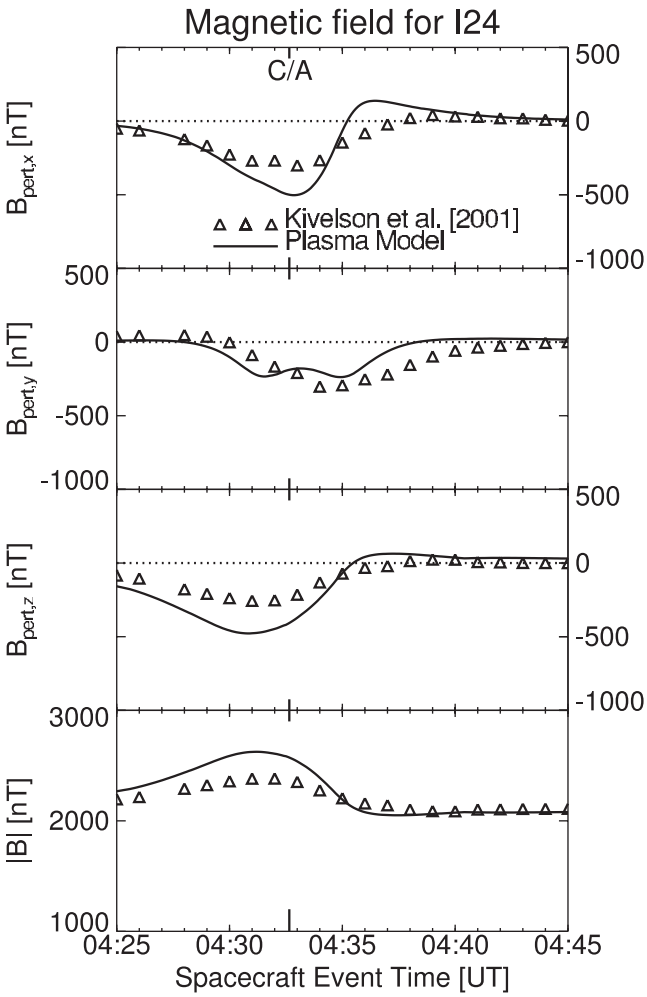

Figure 18. Magnetic field for I24 flyby for longitudinal symmetric atmosphere model. Values are normalized to upstream conditions, respectively.

[39] It is useful to show the results for a longitudinal symmetric atmosphere model (see Figure 18). In this case more electric current flows on the upstream side, which creates a stronger signature in the z component and the magnetic field magnitude than is actually observed by the Galileo spacecraft [*Kivelson et al.*, 2001]. This comparison supports the case for a longitudinally asymmetric atmosphere.

[40] In our model the principal orientation of the x and y components of the magnetic field agree well with the observations. In this region, the magnetic field topology can also be explained nicely by the field line draping picture as done by *Kivelson et al.* [2001].

[41] We underestimate the x and the y components of the magnetic field with our standard model. This might be due in part to problems with the nonuniqueness of coordinate systems used to compare the data with our model results (see discussion in section 2).

3.4. I27 Flyby

[42] The next flyby where plasma and magnetic field data were taken is the I27 flyby. This flyby has a similar trajectory to I24 with closest approach at an altitude of about 300 km (see Figure 2).

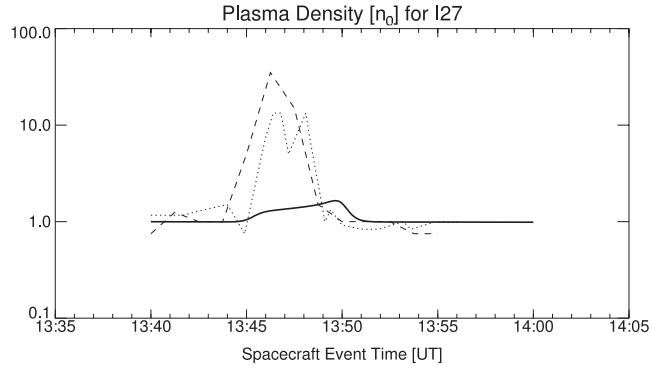

Figure 19. Modeled plasma density for I27 flyby for standard model (solid line) and observed data by *Frank and Paterson* [2001] (dotted line) and *Gurnett et al.* [2001] (dashed line). Values are normalized to upstream conditions, respectively.

3.4.1. Plasma Density and Velocity

[43] In Figure 19 we show the plasma density along the I27 flyby. As can be seen, the Galileo spacecraft passed through Io's ionosphere. We model an increased plasma density by about a factor of two near the closest approach, whereas the observations reported by *Gurnett et al.* [2001] and *Frank and Paterson* [2001] showed a density enhancement by about a factor of ten to thirty. There might be several reasons for this discrepancy. The effectiveness of electron heat conduction along the magnetic field lines determines where the plasma ionization source is strongest, i.e., decreasing effectiveness moves the maxima of the density more downstream. See, for example, Figure 10 by *Saur et al.* [1999] where we assumed an infinite heat conductivity and thus found that the maximum of the plasma density was a factor of 10 enhancement on the upstream side. In addition, we expect strong effects due to multiion chemistry. In particular, a lower recombination rate of atomic ions will enhance the total electron density.

[44] The plasma velocity for the case of the I27 trajectory is significantly slowed by nearly a factor of about ten as we show in Figure 20 and is in agreement with *Frank and*

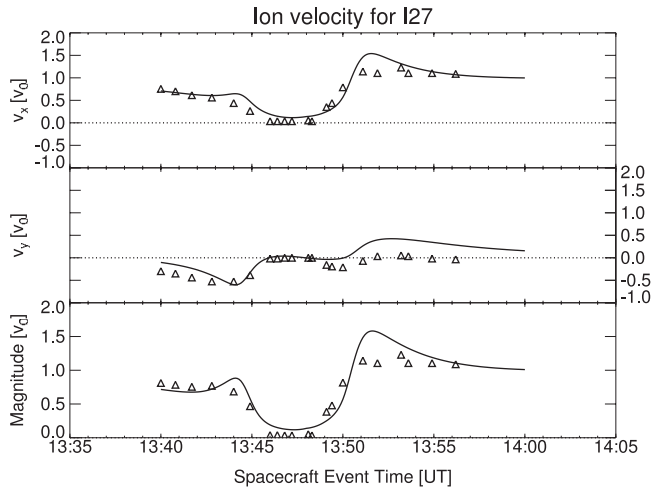

Figure 20. Ion velocity for I27 flyby for standard model, triangles: *Frank and Paterson* [2001]. Values are normalized to upstream conditions, respectively.

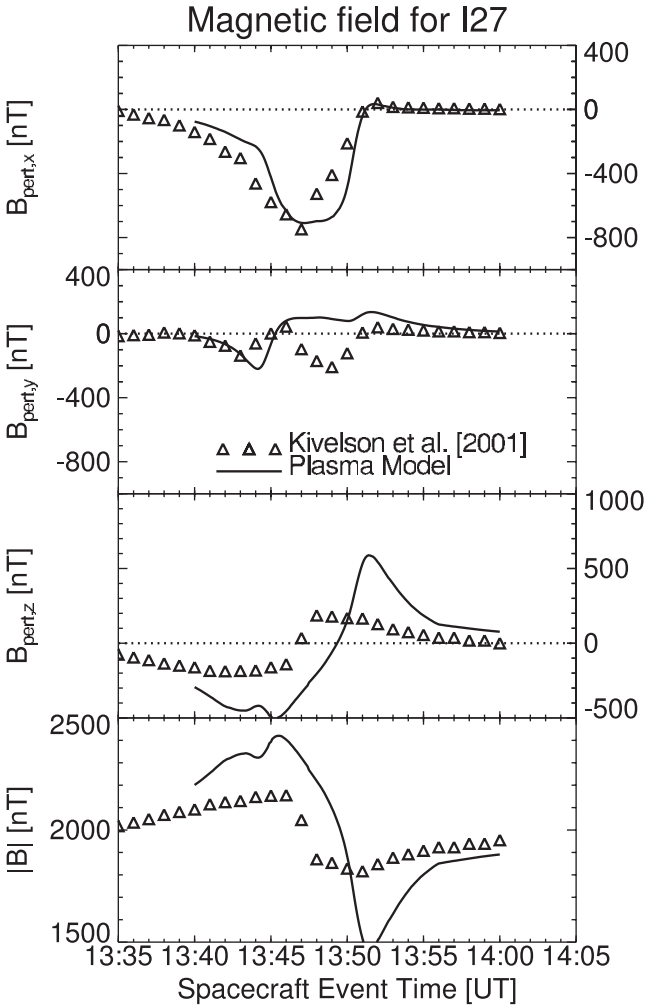

Figure 21. Magnetic field for I27 flyby for standard model.

Paterson [2001]. The x and the y components are typical for a flow that slows and is deflected around an obstacle with the v_y component on the upstream side pointing away from Io, and on the downstream side again toward Io, i.e., the flow closes toward the wake.

3.4.2. Magnetic Field

[45] In Figure 21 we show our magnetic field predictions in comparison to the measurements of *Kivelson et al.* [2001]. Our model reproduces well the general structure of the observed field, i.e., on the upstream side the magnitude is increased and on the downstream side decreased as we would expect from the discussion of the I0 downstream flyby and the basically upstream flyby I24. This is reflected in the z component, which flips sign. However, we clearly overestimate these signatures in our model. We will return to this problem in the next paragraph. The x component of the magnetic field is well reproduced in our model. It comes from both the ionospheric current flowing in direction away from Jupiter on the upstream side and also the parallel currents toward Jupiter on the anti-Jovian side.

[46] Up to now the differences in our model runs have been attributed to different neutral atmosphere models. However, *Gurnett et al.* [2001] and *Frank and Paterson* [2000] reported modified torus conditions for each flyby. For example, with a reduced torus density of 2000 cm^{-3}, which reduces the Alfvén conductances and thus the maximum possible total current, our model yields a depressed magnetic field signature in accordance with the actual observations (See Figure 22).

3.5. Generic Polar Pass

[47] Unfortunately there were no magnetic field and plasma data taken during the I25 southern polar flyby. However, plasma wave measurements are available from which the electron density can be inferred [*Gurnett et al.*, 2001]. There are three future polar flybys: I31, I32 and I33 for which we make predictions in terms of a generic polar path similar to I31. We chose a closest approach at 200 km directly above the north pole with a trajectory along the x axis (see Figure 2). We show results for several numerical models and one analytical model.

3.5.1. Density and Velocity

[48] The plasma density along the generic trajectory (not shown) is only modestly enhanced by about 50%. *Gurnett et al.* [2001] reported a boxcar shaped electron density enhancement of a factor of four above Io's pole during the I25 flyby. Its width is about the size of Io. Our model does not reproduce this feature. Since the atmosphere can

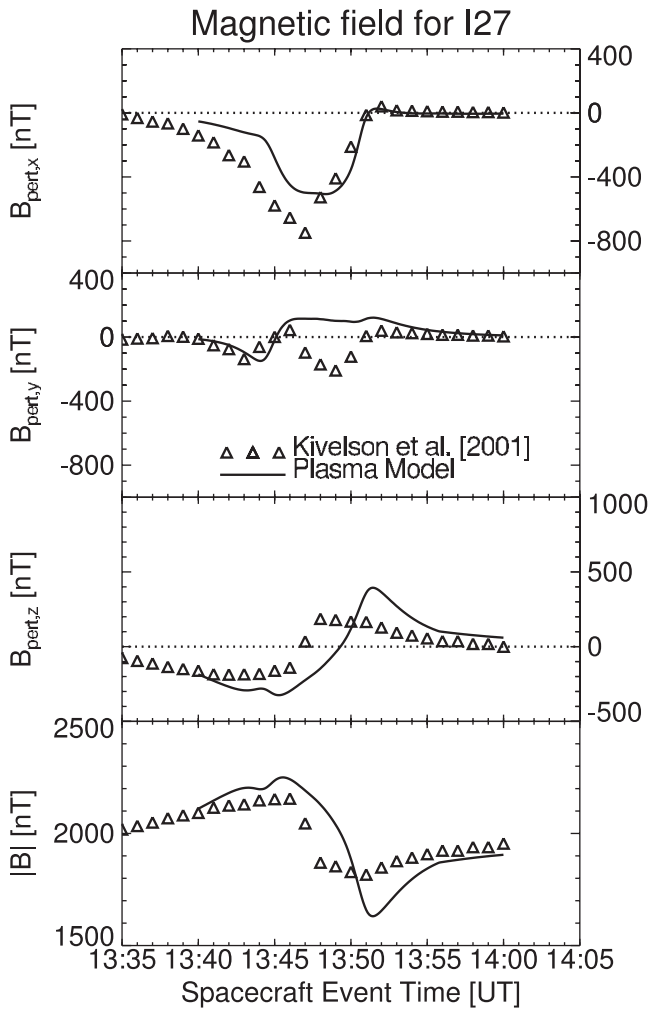

Figure 22. Magnetic field for I27 for standard model, but with upstream torus density of 2000 cm^{-3}.

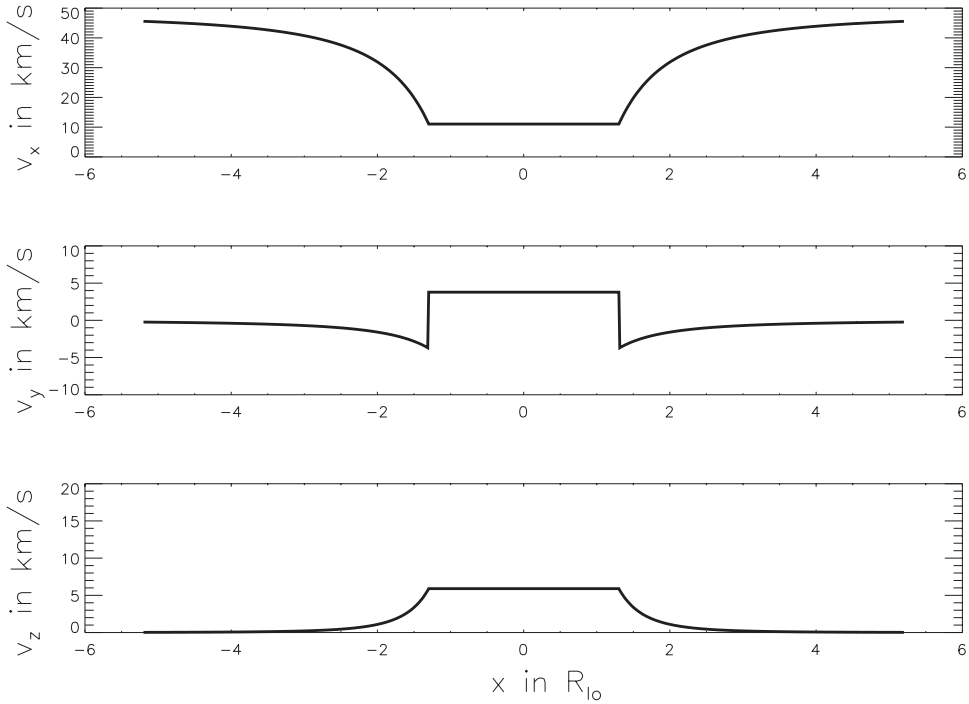

Figure 23. Plasma velocity for generic path through analytically calculated northern Alfvén wing. Note that the inclination of the Alfvén wing by tan $\Theta_A = M_A$ is included in the calculation.

change on small timescales mostly due to its volcanoes, there could have been an enhanced neutral density during this flyby. But more likely the reason might be that we do not solve the velocity equation along the magnetic field. Pressure gradients will transport plasma along the field lines out of Io's ionosphere or into the wake, which is, in this case, related to a possible slow mode wing predicted by several authors, e.g., *Neubauer* [1980] and *Linker et al.* [1991]. The subject has recently been discussed again by *Neubauer* [2000] who showed that kinetic and atomic processes can very effectively produce pressure gradients along the magnetic field which then generate slow waves propagating along the magnetic field with plasma transport inward or outward depending on the precise conditions. These effects will strongly influence densities, pressures, temperatures and the velocity components parallel to the magnetic field, whereas the magnetic field components will be affected to a lesser extent.

[49] Since the polar pass resembles in part a pass through an Alfvén wing, it is instructive to look at an analytic velocity profile (see Figure 23). This is calculated from the Alfvén wing solution of *Neubauer* [1980] where we use for the electric field the analytical solution from *Saur et al.* [1999] that includes the Hall effect. The values of the conductances are $\Sigma_1 = 50$ S and $\Sigma_2 = 50$ S and the radius of the ionosphere was assumed to be 1.3 R_{Io}. We calculate the solution for the northern Alfvén wing and rotate it by the angle θ_A [see *Neubauer*, 1980] in our coordinate system. Note that this is the field of a pure Alfvén wing, where Io's local interaction is assumed to be far away. This is not the case for a flyby at 200 km but it is, nevertheless, useful as a limiting case.

[50] In the Alfvén wing the velocity is reduced. If there were no Hall effect, there would not be an asymmetry between the side of Io facing Jupiter and the opposite side and thus the y component of the velocity should be zero on this trajectory. However, the velocity is rotated toward Jupiter by an angle tan $\Theta_{twist} = \Sigma_2/(\Sigma_1 + 2\,\Sigma_A)$. This angle is derived analytically in the appendix of *Saur et al.* [1999] for the rotation of the local electric field due to the Hall effect. This field maps out into Io's Alfvén wings where the frozen-in-field theorem holds and thus the plasma flow is rotated by the same angle toward Jupiter (Note that in Io's vicinity the frozen-in-field theorem does not hold and thus ideal MHD is not applicable).

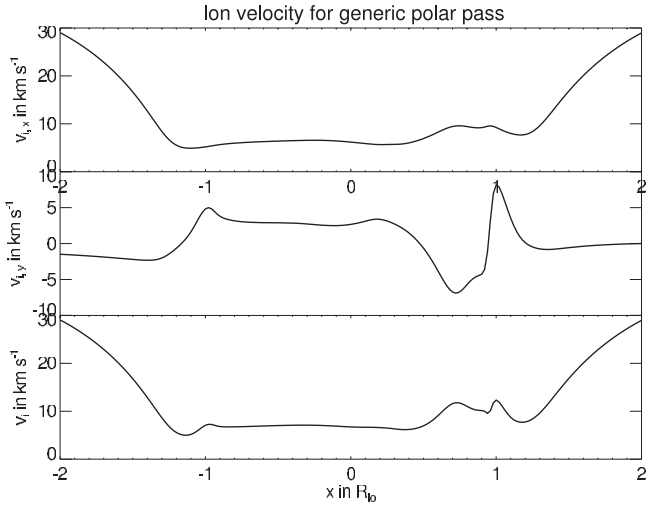

Figure 24. Ion velocity for generic polar path for radially symmetric atmosphere model. Note bottom panel is the magnitude of velocity.

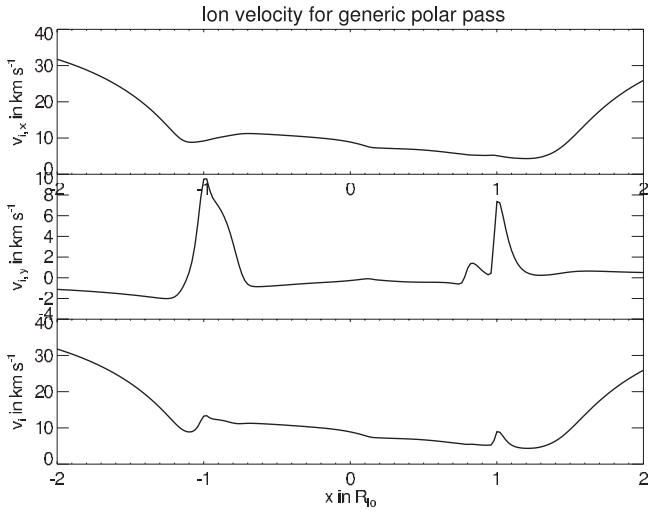

Figure 25. Ion velocity for generic polar path for standard model. Note bottom panel is the magnitude of velocity.

[51] In Figure 24 we show the model velocity with a radially symmetric neutral atmosphere model, where the conductance distribution still resembles the analytic solution by *Saur et al.* [1999]. It can be seen, as for the analytic solution, that the velocity is slowed and rotated.

[52] For the latitudinally asymmetric atmosphere we show the velocity in Figure 25. In this case there is very little atmosphere above the poles and thus also very small Hall conductances. Therefore the flow is rotated toward Jupiter only on field lines that map to equatorial regions with high neutral density, and thus also high Hall conductivities. This is evident in the two peaks in the *y* component of the velocity.

3.5.2. Magnetic Field

[53] Now we discuss the magnetic field along our generic polar path. We show the magnetic field for the same three scenarios as for the velocities above, in Figures 26, 27, and 28. All three have in common a strong component toward the negative *x* direction, which is the strongest feature of the Alfvén wing perturbation. Without the Hall effect there would be no perturbation field in the *y* direction with the assumed symmetries in our atmosphere models. However, due to the Hall effect, the analytic magnetic field solution is rotated from the unperturbed direction by the same angle Θ_{twist} as is the velocity. This rotation can also be seen in our numerical model with the

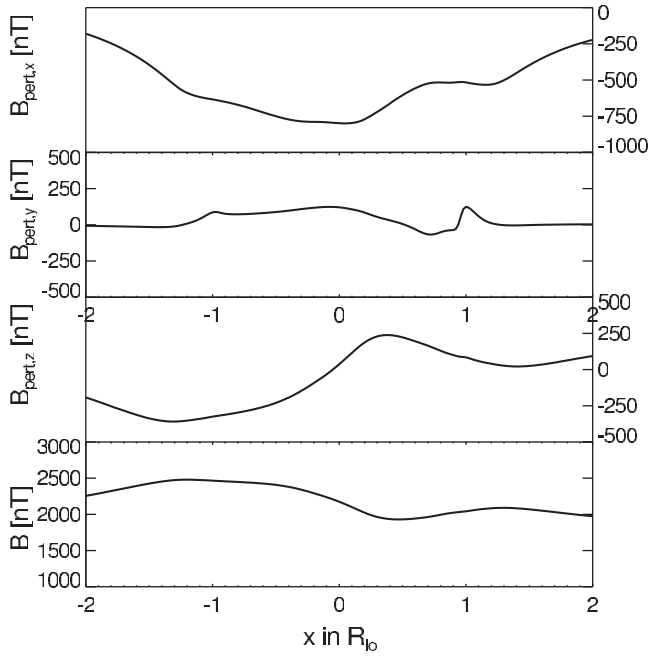

Figure 27. Magnetic field for generic polar path with radially symmetric atmosphere model.

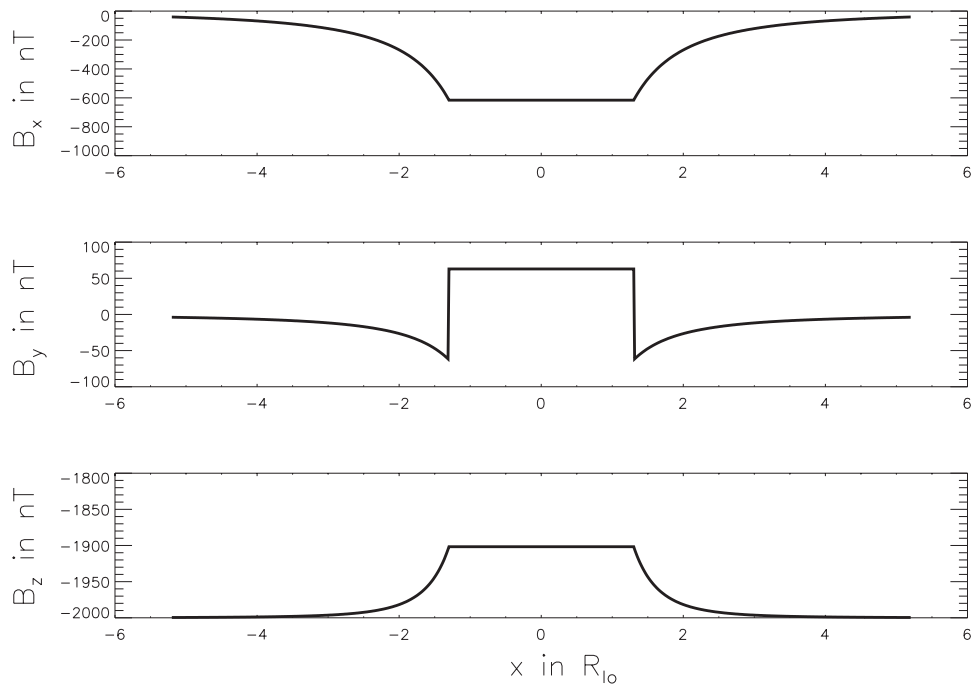

Figure 26. Magnetic field for generic polar path through analytically calculated Alfvén wing.

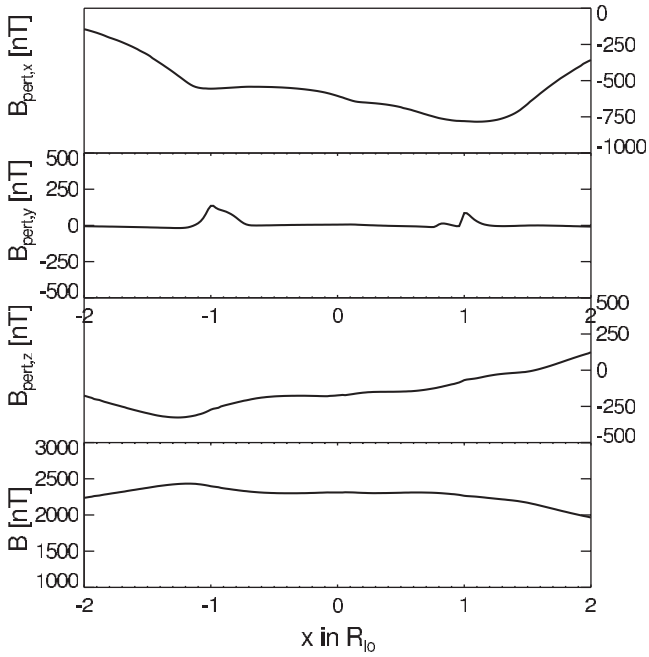

Figure 28. Magnetic field for generic polar path for standard model.

radially symmetric neutral atmosphere (see Figure 27). As for the velocity in the case of the longitudinally and latitudinally asymmetric atmosphere model, this rotation is the least visible, but can be still seen in the two peaks in the y direction toward Jupiter.

[54] The z component of the field is weakly disturbed. In both numerically modeled cases the negative values on the upstream and the positive component on the downstream side are effects of the strong equatorial ionospheric current system which flows on the upstream and downstream side around Io. In the exact solution of *Neubauer* [1980] the constant magnitude of the field is a basic property of the Alfvén wing. We note that the magnetic field and the velocity components behave very similar as expected for an Alfvén wing pass, where one expects the Alfvén relationship $\delta\mathbf{B}/\sqrt{\mu_0\rho_0} = \mp\delta\mathbf{v}$. The negative sign corresponds to propagation along the magnetic field, and thus corresponds to the southern hemisphere. The positive sign is for the opposite direction of propagation, i.e., the northern Alfvén wing, for which we present results (see Figures 23–28). This relationship can on the other hand be used to check how "pure" Alfvénic the farfield interaction of Io actually is (see the discussion by *Crary and Bagenal* [1997] or *Neubauer* [1998a]). This question might be also addressed by estimating the total electric current in each polar flyby. An Alfvénic interaction should depend on the Alfvén conductance and thus on the torus density of each flyby.

[55] This polar trajectory is well suited to learn about Io's interaction. If Io has an internal magnetic field of the magnitude and orientation proposed by *Kivelson et al.* [1996a, 1996b], then a very strong signature in the z direction is created, whereas in the absence of an internal field only a small perturbation is generated. Also the signature in the x component of the field is significantly different in the internal or no-internal field case. An internal magnetic field basically does not produce a perturbation in this direction, whereas the Alfvénic signature would be very prominent (see Figures 26, 27, and 28).

[56] Observations along this trajectory should yield information about Io's atmosphere, especially from the observation of the degree of rotation of the fields and the flow. These quantities constrain the atmospheric neutral density and the location of the rotation gives insight on the neutral atmosphere distribution, e.g., whether and where there is significant polar neutral atmosphere.

4. Summary and Discussion

[57] Our updated 3D plasma two-fluid model is able to reproduce the salient features of the Galileo Io flyby I0 in December 1995, I24 in October 1999 and I27 in February 2000. In particular, we can reproduce the Galileo spacecraft magnetic field observations [*Kivelson et al.*, 1996a, 1996b, 2001] without the assumption of an internal magnetic field of Io. However, these flybys do not unambiguously resolve the question whether Io has an internal magnetic field and thus a polar flyby is required to resolve this issue. Therefore we predict magnetic field and plasma properties for a generic polar pass which should help distinguish between magnetic field perturbations generated from an internal field and those generated by parallel Alfvén and ionospheric currents due to plasma interaction with Io's atmosphere and ionosphere. We also present an interpretation of the double-peak structure in the I0 magnetic field observations due to diamagnetic and inertia currents.

[58] We also give evidence that Io's neutral atmosphere is not longitudinally symmetric, i.e., it is squeezed on the upstream side and stretched on the downstream side due to the drag force of the torus plasma on the neutral atmosphere. Thus we expect a smaller neutral scale height on the upstream side than on the downstream side. This drag force is also the origin of Io's electrodynamic interaction, i.e., it is balanced by the j $\times$ B force with a current that carries about 10 Million A through Io's atmosphere.

[59] The bidirectional electrons might play an important role for the formation of Io's downstream ionosphere. Finally we note that a polar pass might provide unique information on the formation of slow magneto-acoustic waves and wings and also useful information about the distribution of Io's atmosphere, especially from rotated Alfvén wings.

Appendix A. Heat Equations

[60] In this appendix we present the explicit form of our model electron equation with its derivation and underlying simplifying assumptions. The one-dimensional electron heat equation along the magnetic field lines is given, following, for example, *Banks and Kockarts* [1973], by

$$3/2k_B n_e \frac{dT_e}{dt} = -\frac{\partial Q_{\text{flux}}}{\partial z} - 3/2k_B T_e\left(f_{\text{ion}}(T_e)n_e + k_{\text{ph}} + k_{\text{he}}\right)n_n - \left(\mathcal{L}(T_e)n_e - \mathcal{K}_{\text{ph}}\right)n_n + f_{\text{heating}} \quad \text{(A1)}$$

with the electron temperature T_e, the Boltzmann constant k_B, the heat flux Q_{flux}, the electron impact ionization rate f_{ion},

the photoionization rate $k_{\rm ph}$, the ionization rate due to the high energetic electrons $k_{\rm he}$, the energy loss rate due to inelastic collisions $\mathcal{L}$, the heating rate due to photoionization $\mathcal{K}_{\rm ph}$, and the heating rate $f_{\rm heating}$ due to collisions with ions and neutrals at lower temperatures. Detailed expressions for each term are given by *Saur et al.* [1999].

[61] Now we separate each flux tube into two regions with two different electron temperatures, i.e., Io's ionosphere with the temperature T_e^I and the Io plasma torus with the temperature T_e^T. For the ionospheric region we assume a lower boundary at R_d and the upper boundary at R_a. The torus region ranges from R_a to an upper boundary $R_{\rm u}$, which we assume to be the torus boundary $R_{\rm Torus}$. Since we assume that the electron temperature is constant within each region, the ionospheric and the torus temperature can be derived by integration of (A1) along a flux tube within each region. For the ionospheric temperature we integrate (A1) from the lower boundary R_d to the upper boundary R_a. The lower boundary is the equatorial plane given by $z = 0$, the surface of Io, or in the wake the lowest height where there is still plasma. The upper boundary R_a is placed at Io's ionosphere (or atmosphere) boundary, which we assume be a shell of radius $2.4 \times R_{\rm Io}$. In this way, we find for the ionospheric temperature

$$\frac{d}{dt}T_e^I = -\left[\int_{R_d}^{R_a} n_e dz\right]^{-1}\left[\frac{2}{3k_B}Q_{\rm flux}(R_a) + \left[1 - G\left(T_e^I\right)\right]\cdot\left[\left(\left(T_e^I f_{\rm ion} + \frac{2}{3k_B}\mathcal{L}\right)\int_{R_d}^{R_a} N n_n dz + \int_{R_d}^{R_a} n_n\left(T_e^I\left(k_{\rm ph} + k_{\rm he}\right) - \frac{2}{3}\mathcal{K}_{\rm ph}/k_B\right)dz\right]\right] \tag{A2}$$

We assume that the heat flux $Q_{\rm flux}(R_d)$ at lower boundary R_d vanishes. For $R_d = 0$ this is true for symmetry reasons, and when the lower boundary R_d is the surface of Io then we expect a thick neutral atmosphere boundary layer directly above Io's surface with a small neutral scale height (see, e.g., *Strobel et al.* [1994]), which prevents a significant heat flux into Io. We adjusted the heating term $f_{\rm heating}$ for small temperatures with a phenomenological introduction of

$$G\left(T_e^I\right) = \begin{cases} 1 & \text{for} \quad T_e^I < 0.2eV \\ \exp\left\{-\left(\left(T_e^I - 0.2eV\right)/T_{\rm width}\right)^2\right\} & \text{for} \quad T_e^I \geq 0.2eV \end{cases} \tag{A3}$$

With this choice, we ensure that the cooling is balanced by the reverse heating when the electron temperature approaches the neutral atmosphere temperature of 0.2 eV. For more details see *Saur et al.* [1999] or *Saur* [2000].

[62] For the evolution equation for the electron temperature in the torus we proceed in the same manner and integrate (A1) within the torus from the lower boundary R_a to the upper torus boundary $R_{\rm u} = R_{\rm Torus}$. In this region with no neutral atmosphere most of the sources and sinks in (A1) vanish and we get simply

$$\frac{d}{dt}T_e^T = \frac{Q_{\rm flux}(R_a)}{3/2k_B(R_{\rm u} - R_a)n_{e,0}} \tag{A4}$$

This equation describes how the energy reservoir, Io plasma torus, loses its energy due to heat flux from the torus into Io's ionosphere.

[63] Finally we now describe how we parameterize the heat flux that controls the amount of energy that is conducted from the Io plasma torus into Io's ionosphere. In general the heat flux is given by

$$Q_{\rm flux} = -\kappa\frac{\partial}{\partial z}T_e \tag{A5}$$

with the electron heat conductivity given by *Bank and Kockarts* [1973]

$$\kappa = \frac{7.7 \times 10^5}{1 + 3.22 \times 10^3 T_e^2 \sigma_{\rm en} n_n/n_e}\left[\frac{\rm eV}{\rm cm\ s\ K}\right] \tag{A6}$$

For our description we need an average heat flux generated by the temperature gradient from the torus to the ionosphere for which we write

$$\langle Q_{\rm flux}\rangle = \langle\kappa\rangle\frac{T_e^T - T_e^I}{R_{\rm typ}} \tag{A7}$$

with a typical scale height $R_{\rm typ}$ for the heat conduction. In our model we can use $R_{\rm typ}$ to control the strength of the heat flux. We chose as a typical scale $R_{\rm typ} = R_{\rm Io}/2$. However, there is no obvious way to determine the average heat conductivity $\langle\kappa\rangle$, since it is very nonlinear and can vary by orders of magnitude. We choose, quite arbitrarily, to describe the heat flux with the value of κ at R_d, i.e., at the location where the neutral atmosphere is the densest until a given density limit is reached. We like to stress that this approach has to be considered as a way to parameterize the heat flux so that energy is conserved and some desired features for the heat transport in Io's ionosphere are obtained. In the limit of small neutral densities the neutral density has no impact on the heat flux since the second term in the denominator of (A6) is small, i.e., less than one. If the electron flux tubes penetrate denser parts of the neutral atmosphere the heat conductivity decreases, and thus heat flux from the torus is slowed down in comparison to an infinite heat conductivity. For flux tubes that penetrate Io's very dense atmosphere this approach probably seriously underestimates the average heat flux, since the denominator in (A6) is evaluated at the densest part of the atmosphere and is thus very large and the heat conductivity very small. However, away from this density maximum the heat conductivity rapidly increases along the flux tube. Thus we decided again, quite arbitrarily, if the second term $T2$ ($= 3.22 \times 10^4 T_e^2 \sigma_{\rm en} n_n/n_e$) in the denominator of (A6), which competes with 1 in this denominator, is larger than a special

value $T2_{max}$, we do not increase it anymore but keep T2 = $T2_{max}$. We used $T2_{max}$ = 1000. In this way we make sure that there is still some energy flux in this flux tube since in the upper part of the flux tube the neutral density is small.

[64] **Acknowledgments.** We appreciate that M. Kivelson and her team provided us with magnetic field data of the Galileo Io flybys I0, I24 and I27 in advance of publications. Also thanks are due to C. Neimöck who prepared Figures 1 and 12 and A. Kassner for providing plot software for the numerical output. J. S. and F. M. N. acknowledge support by the Deutsche Forschungsgemeinschaft and DLR to a lesser extend. D. F. S. and J. S., partially, were supported by NASA Grant NAG5-4168.

References

Banks, P. M., and G. Kockarts, *Aeronomy*, vol. A, Academic, San Diego, Calif., 1973.

Baumjohann, W., and R. A. Treumann, *Basic Space Plasma Physics*, Imperial College Press, London, 1996.

Combi, M. R., K. Kabin, T. I. Gombosi, D. L. De Zeeuw, and K. G. Powell, Io's plasma environment during the Galileo flyby: Global three-dimensional MHD modeling with adaptive mesh refinement, *J. Geophys. Res.*, *103*, 9071–9081, 1998.

Crary, F. J., and F. Bagenal, Coupling the plasma interaction at Io to Jupiter, *Geophys. Res. Lett.*, *24*, 2135–2138, 1997.

Feldman, P. D., et al., Lyman-alpha imaging of the SO_2 distribution on Io, *Geophys. Res. Lett.*, *27*, 1787–1790, 2000.

Frank, L. A., and W. R. Paterson, Intense electron beams observed at Io with the Galileo spacecraft, *J. Geophys. Res.*, *104*, 28,657–28,669, 1999.

Frank, L. A., and W. R. Paterson, Return to Io by the Galileo spacecraft: Plasma observations, *J. Geophys. Res.*, *105*, 25,363–25,378, 2000.

Frank, L. A., and W. R. Paterson, Passage through Io's inonospheric plasmas by the Galileo spacecraft, *J. Geophys. Res.*, *106*, 26,209–26,224, 2001.

Frank, L. A., W. R. Paterson, K. L. Ackerson, V. M. Vasyliunas, F. V. Coroniti, and S. J. Bolton, Plasma observations at Io with the Galileo spacecraft, *Science*, *274*, 394–395, 1996.

Gurnett, D. A., W. S. Kurth, A. Roux, S. J. Bolton, and C. F. Kennel, Galileo plasma wave observations in the Io plasma torus and near Io, *Science*, *274*, 391–392, 1996.

Gurnett, D. A., A. Persoon, and W. Kurth, Electron densities near Io from Galileo plasma wave observations, *J. Geophys. Res.*, *106*, 26,225–26,232, 2001.

Hinson, D. P., A. J. Kliore, F. M. Flasar, J. D. Twicken, P. J. Schindler, and R. G. Herrera, Galileo radio occultation measurements of Io's ionosphere and plasma wake, *J. Geophys. Res.*, *103*, 29,343–29,358, 1998.

Kabin, K., M. R. Combi, T. I. Gombosi, D. L. DeZeeuw, K. C. Hansen, and K. G. Powell, Io's magnetospheric interaction: An MHD model with day–night asymmetry, *Planet. Space Sci.*, *49*, 337, 2001.

Khurana, K. K., M. G. Kivelson, and C. T. Russell, Interaction of Io with its torus: Does Io have an internal magnetic field?, *Geophys. Res. Lett.*, *24*, 2391–2394, 1997.

Kivelson, M. G., K. K. Khurana, R. J. Walker, C. T. Russell, J. A. Linker, D. J. Southwood, and C. Polanskey, A magnetic signature at Io: Initial report from the Galileo magnetometer, *Science*, *273*, 337–340, 1996a.

Kivelson, M. G., K. K. Khurana, R. J. Walker, J. Warnecke, C. T. Russell, J. A. Linker, D. J. Southwood, and C. Polanskey, Io's interaction with the plasma torus: Galileo magnetometer report, *Science*, *274*, 396–398, 1996b.

Kivelson, M. G., et al., Magnetized or unmagnetized: Ambiguity persists following Galileo's encounters with Io in 1999 and 2000, *J. Geophys. Res.*, *106*, 26,121–26,135, 2001.

Kliore, A. J., G. Fjeldbo, B. L. Seidel, D. N. Sweetnam, T. T. Sesplaukis, P. M. Woiceshyn, and S. I. Rasool, The atmosphere of Io from Pioneer 10 radio occultation measurement, *Icarus*, *24*, 407–410, 1975.

Linker, J. A., M. G. Kivelson, and R. J. Walker, A three-dimensional MHD simulation of plasma flow past Io, *J. Geophys. Res.*, *96*, 21,037–21,053, 1991.

Linker, J. A., K. K. Khurana, M. G. Kivelson, and R. J. Walker, MHD simulations of Io's interaction with the plasma torus, *J. Geophys. Res.*, *103*, 19,867–19,877, 1998.

Neubauer, F. M., Nonlinear standing Alfvén wave current system at Io: Theory, *J. Geophys. Res.*, *85*, 1171–1178, 1980.

Neubauer, F. M., The sub-Alfvénic interaction of the Galilean satellites with the Jovian magnetosphere, *J. Geophys. Res.*, *103*, 19,843–19,866, 1998a.

Neubauer, F. M., Comment on "Interaction of Io with its torus: Does Io have an internal magnetic field?" by Krishan K. Khurana, Margaret G. Kivelson and Christopher T. Russell, *Geophys. Res. Lett.*, *25*, 2349–2350, 1998b.

Neubauer, F. M., On the plasma distribution in the polar regions of the Galilean satellites, particularly Io: Field-aligned plasma motion, *Eos Trans. AGU*, *81*(48), Fall Meet. Suppl. P62D-05, 2000.

Roesler, F. L., et al., Far-ultraviolet imaging spectroscopy of Io's atmosphere with HST/STIS, *Science*, *283*, 353–357, 1999.

Saur, J., Plasma interaction of Io and Europa with the jovian magnetosphere, Dissertation, Inst. für Geophys. und Meteorol. der Univ. zu Köln, Cologne, Germany, 2000.

Saur, J., F. M. Neubauer, D. F. Strobel, and M. E. Summers, Three-dimensional plasma simulation of Io's interaction with the Io plasma torus: Asymmetric plasma flow, *J. Geophys. Res.*, *104*, 25,105–25,126, 1999.

Saur, J., F. M. Neubauer, D. F. Strobel, and M. E. Summers, Io's ultraviolet aurora: Remote sensing of Io's interaction, *Geophys. Res. Lett.*, *27*, 2893–2896, 2000.

Strobel, D. F., and B. C. Wolven, The atmosphere of Io: Abundance and sources of sulfur dioxide and atomic hydrogen, *Astrophys. Space Sci.*, *277*, 271–287, 2001.

Strobel, D. F., X. Zhu, and M. E. Summers, On the vertical thermal structure of Io's atmosphere, *Icarus*, *111*, 18–30, 1994.

Thorne, R. M., D. J. Williams, L. D. Zhang, and S. Stone, Energetic electron butterfly distributions near Io, *J. Geophys. Res.*, *104*, 14,755–14,766, 1999.

Williams, D. J., et al., Electron beams and ion composition measured at Io and in its torus, *Science*, *274*, 401–403, 1996.

Williams, D. J., R. M. Thorne, and B. Mauk, Energetic electron beams and trapped electrons at Io, *J. Geophys. Res.*, *104*, 14,739–14,753, 1999.

F. M. Neubauer, Institut für Geophysik und Meteorologie, Albertus Magnus Platz, 50923 Köln, Germany. (neubauer@geo.uni-koeln.de)

J. Saur and D. F. Strobel, Departments of Earth and Planetary Sciences and Physics and Astronomy, Johns Hopkins University, Baltimore, MD 21218, USA. (saur@jhu.edu; strobel@jhu.edu)

M. E. Summers, School of Computational Sciences and Dept. of Physics and Astronomy, George Mason University, Fairfax, VA, USA. (msummers@physics.gmu.edu)